The auditory midbrain mediates tactile vibration sensing

Erica L. Huey[1,2], Josef Turecek[1,2], Michelle M. Delisle[1,2], Ofer Mazor[1], Gabriel E. Romero[1], Malvika Dua[1,2], Zoe K. Sarafis[1,2], Alexis Hobble[1,2], Kevin T. Booth[1], Lisa V. Goodrich[1], David P. Corey[1], and David D. Ginty[1,2]

[1]Department of Neurobiology, [2]Howard Hughes Medical Institute, Harvard Medical School, 220 Longwood Avenue, Boston, MA 02115

Correspondence: david_ginty@hms.harvard.edu

Summary

Vibrations are ubiquitous in nature, shaping behavior across the animal kingdom. For mammals, sound waves traveling through air are captured by the cochlea and the neural signals they generate are encoded in the auditory system[1]. Mechanical vibrations acting on the body are detected by mechanoreceptors of the skin and deep tissue and processed by the somatosensory system[2]. As such, the neural pathways that underlie perception and reaction to sound waves and mechanical vibrations are believed to be anatomically distinct and functionally independent. Here, we report that mechanical vibrations are prominently encoded by neurons in the lateral cortex of the inferior colliculus (LCIC) of the auditory midbrain. LCIC responses to environmental vibrations are mediated by Aβ rapidly adapting (RA)-LTMRs associated with Pacinian corpuscles, which are exquisitely sensitive and unique in their ability to entrain to high - frequency (40-1000 Hz) environmental vibrations[2-5]. Remarkably, most LCIC neurons are dual somatosensory and auditory environmental vibration detectors. Moreover, the LCIC is required for behavioral responses to high frequency mechanical vibrations, but not other somatosensory modalities. Thus, environmental vibrations captured by Pacinian corpuscles of the body are encoded in the auditory midbrain to mediate behavior.

Main text

Vibration sensing is ubiquitous across the animal kingdom, enabling organisms to interpret their dynamic surroundings, communicate, detect threats, and navigate their environment[6-10]. In mammals, vibrations that propagate through the air in the form of sound waves are transduced into electrical signals in the cochlea and encoded by the auditory system[1]. Analogously, mechanical vibrations acting on the body are detected by fast conducting low-threshold mechanoreceptors (Aβ LTMRs) of the body and encoded by the somatosensory system[2,11]. In many animals, including humans, the vibration frequency detection range of the auditory system (20 Hz-20 kHz) partially overlaps with that of the somatosensory system (1-1000 Hz)[2,12-14]. In some smaller mammals, such as mice, the encoding of vibration frequency in the somatosensory system (1-1000 Hz) and auditory system (~1 khz-100 kHz) is largely non-overlapping[5,12,13,15-17].

Our understanding of LTMRs and their role in detecting mechanical vibrations mainly arises from experiments in which vibratory stimuli are presented directly to the body; however, the somatosensory system can also detect subtle, low amplitude environmental vibrations. In a noteworthy example, elephants can communicate over miles, sensing vocalizations and movements of conspecifics by detecting vibrations of the ground using mechanoreceptors in their feet and trunks[9,18]. Among the LTMRs, Pacinian corpuscle Aβ rapidly adapting type-2 (RA2)-LTMRs are unique in their capacity to encode high frequency vibrations[2]. In humans and primates, Pacinians are located in the deep dermis of glabrous skin and also associated with joints and connective tissue[19,20]. In rodents, Pacinians are enriched in the periosteum of wrist and ankle bones, rendering them responsive to vibrations transmitted through the skeleton[2,5,16,21,22]. Recordings from Pacinian afferents in awake, behaving mice have recently revealed their exquisite sensitivity to self-movements and substrate vibrations under naturalistic conditions[5]. Indeed, Pacinian corpuscle Aβ RA2-LTMRs can fire robustly in response to low-amplitude environmental vibrations, including those initiated by gentle movements on surfaces located meters from where an animal stands[5,23-26].

The canonical view is that the neural impulses encoding mechanical vibrations of the body are conveyed via the brainstem dorsal column nuclei (DCN) to the ventroposterolateral thalamus (VPL) *en route* to primary somatosensory cortex (S1)[11,27]. However, recent work suggests that

high frequency vibration sensitive DCN neurons project to the inferior colliculus, a midbrain region involved in auditory information processing[1,28]. The inferior colliculus (IC) is comprised of multiple subregions: the central nucleus of the inferior colliculus (CNIC), which solely receives auditory input in a tonotopic manner, and the lateral cortex of the inferior colliculus (LCIC), which receives inputs from multiple sensory modalities, including somatosensory inputs from the DCN (Fig. 1A, Extended Data Fig. 1)[1,28-39]. Here, we use electrophysiological recordings, genetic manipulations, and behavioral analyses to show that most LCIC neurons encode both high frequency mechanical vibrations captured by Pacinian corpuscle LTMRs and auditory vibrations captured by the cochlea to mediate behavioral responses to environmental vibrations.

LCIC and VPL neurons are differentially tuned to mechanical vibrations

Distinct populations of DCN neurons send axonal projections to either the VPL or the LCIC (Fig. 1A, Extended Data Fig. 1)[38]. To compare how mechanical vibrations are represented in the LCIC and VPL, we performed *in vivo* multi-electrode array (MEA) recordings in these brain regions in urethane anesthetized animals (Extended Data Fig. 2). We first brushed the animal to identify neurons containing limb receptive fields. Sinusoidal mechanical vibrations of different frequencies and amplitudes were then delivered to the limbs using a mechanical stimulator. While the LCIC and VPL both contain forelimb- and hindlimb-responsive neurons (Extended Data Fig. 2, Extended Data Fig. 3), we focused primarily on hindlimb responsive neurons. Vibrations were delivered to the most responsive region, or "hotspot," of a neuron's receptive field. In the VPL, vibratory receptive fields tended to be focal areas such as an individual pad or digit (Fig 1C). In contrast, receptive fields of LCIC neurons lacked a focal hotspot and were spatially extensive (Fig. 1E). In these cases, the mechanical stimulator was positioned on the heel of the hindlimb. Vibratory stimuli were then delivered at frequencies between 10-900 Hz and forces between 2-50 mN. The majority of VPL neurons responded robustly to low frequency vibrations (<200 Hz), but only transiently to high frequency vibrations (>200 Hz; Fig. 1B, Extended Data Fig. 2C-D, Extended Data Fig. 5A,E). While their pre-synaptic DCN inputs were able to entrain (phase-lock firing to each cycle of the stimulus) to vibratory frequencies up to 100 Hz[18], no VPL neurons could entrain up to 100 Hz, although some neurons could entrain to vibratory frequencies up to 50 Hz. Strikingly, LCIC neurons showed an inverse response pattern

compared to VPL neurons, with most neurons responding transiently to low frequency vibrations (<200 Hz) but firing robustly to high frequency stimuli (200-900 Hz; Fig. 1D, Extended Data Fig. 2G-H, Extended Data Fig. 5I,M). While many DCN projection neurons targeting the LCIC entrained to vibratory frequencies from 10-500 Hz[18], LCIC neurons only transiently responded to low frequency stimuli (Fig. 1D, S2G-H, Extended Data Fig. 5I), suggesting a synaptic filtering mechanism between the DCN and LCIC that preferentially favors high frequency vibratory stimuli. Furthermore, although LCIC neurons responded robustly to high frequency vibrations, they exhibited little or no entrainment (Fig. 1D, Extended Data Fig. 2G-H, Extended Data Fig. 5M).

While high frequency vibratory responses were abundant throughout the LCIC, the sparsity of high frequency responses detected in the VPL was surprising and could be attributed to missing a potential "high frequency hotspot" region in the VPL in our recordings. Therefore, considering that the VPL is an elongated structure extending along the anterior-posterior axis of the brain, we next used a four shanked MEA to perform a detailed mapping of somatotopy across the VPL to search for high frequency vibratory responses. We recorded from a minimum of 9 penetrations per animal using the four-shanked probe, enabling sampling across at least 36 regions of the VPL, distributed across the medio-lateral and anterio-posterior axes. The resulting somatotopic map of the VPL aligned well with those previously reported, with receptive fields moving from forelimb to hindlimb to trunk, when moving from medial to lateral within the VPL (Extended Data Fig. 3A, C-D)[40-43]. For VPL neurons with brush responses to hindbody regions, high frequency vibration of the hindlimb activated ~9 percent of neurons, and these high frequency responsive neurons were sparsely distributed throughout the VPL, not concentrated in a particular subregion (Fig. 1H, Extended Data Fig. 3E). In contrast, >75 percent of brush responsive LCIC neurons responded robustly to high frequency vibrations, indicating that high frequency vibratory information is particularly salient in the LCIC (Fig. 1H).

To assess the relationship between mechanical force thresholds and vibration frequency in the VPL and LCIC, we next obtained force-frequency tuning curves for vibration sensitive VPL and LCIC neurons by determining force thresholds for individual neurons across a range of vibratory frequencies. The force threshold for a given frequency was defined as the minimum force

required to elicit 20 percent of a neuron's maximum firing rate. The tuning curves for VPL and LCIC neurons were approximately U-shaped, although the most sensitive regions of their respective tuning curves were non-overlapping: VPL neurons had the lowest force thresholds to vibrations between 50-200 Hz and LCIC neurons had the lowest force thresholds to vibrations between 300-500 Hz (Fig. 1F-G, I-K). Thus, most LCIC neurons are activated by high frequency vibratory stimuli and exhibit expansive receptive fields, while most VPL neurons are preferentially activated by low frequency stimuli in a spatially restricted manner.

LCIC vibration responses are mediated by Pacinian corpuscle Aβ RA2-LTMRs

The distinct frequency tuning curves and receptive field properties of VPL and LCIC neurons prompted us to ask whether these brain regions receive inputs from different primary mechanosensory neuron types. Rapidly adapting Aβ LTMRs exhibit distinct force-frequency tuning relationships and receptive fields. Most rapidly adapting LTMRs are sensitive to low frequency vibratory stimuli (40-150 Hz) and exhibit relatively small receptive fields[2,11,15,44-46]. This includes Meissner corpuscle Aβ RA1-LTMRs, enriched in glabrous skin of pedal pads and digits, hair follicle Aβ RA-LTMRs associated with body hairs, and Krause corpuscle Aβ RA-LTMRs of the genitalia[2,15,45,47]. In contrast, Pacinian corpuscle Aβ RA2-LTMRs, which in mice are enriched in the periosteum of ankle and wrist bones, are most sensitive to high frequency vibratory stimuli (50-1000 Hz) and have extremely large receptive fields[4,5,21,48-52]. To directly compare the tuning of Meissner corpuscle Aβ RA1-LTMRs and Pacinian corpuscle Aβ RA2-LTMRs to VPL and LCIC neurons, we performed *in vivo* extracellular recordings of DRG neurons and measured force-frequency tuning curves of Meissner and Pacinian afferents (Fig. 1L-N). As predicted, the force-frequency tuning curves of Pacinian corpuscle Aβ RA2-LTMRs resembled those of LCIC neurons, while the tuning curves of Meissner corpuscle Aβ RA1-LTMRs more closely resembled VPL neurons (Fig. 1L-N). These findings led us to hypothesize that Pacinian afferents have an outsized role in shaping the response properties of most LCIC neurons, while Meissner corpuscle afferents and other Aβ RA-LTMRs of the body preferentially contribute to the response properties of most VPL neurons.

149 To directly test the relationship between primary sensory neuron activity and vibration tuning in
150 the LCIC and VPL, we utilized mouse genetic tools to assess the contributions of Pacinian
151 corpuscles and Meissner corpuscles to LCIC and VPL responses. Ret signaling in somatosensory
152 neurons is necessary for formation of Pacinian corpuscles, and thus *Avil*^{Cre}*; Ret*$^{floxGFP/floxGFP}$ (Ret
153 cKO) mice, which lack *Ret* in DRG neurons, lack Pacinian corpuscles (Fig. 2B, Extended Data
154 Fig. 4F)[53,54]. Conversely, TrkB signaling is necessary for formation of Meissner corpuscles, and
155 thus *Avil*^{Cre}*; TrkB*$^{flox/flox}$ (TrkB cKO) mice lack Meissner corpuscles (Fig. 2A)[15,45,55]. Importantly,
156 Ret cKO mice have a normal density of Meissner corpuscles and TrkB cKO mice have a normal
157 density of Pacinian corpuscles (Extended Data Fig. 4).
158
159 Surprisingly, VPL neurons recorded in TrkB cKO and Ret cKO mice showed no notable shifts in
160 their vibration tuning curves (Fig. 2C, F). Meissner corpuscle and Pacinian corpuscle afferents
161 are not the only primary sensory neurons responsive to vibrations, and indeed Aβ RA-LTMRs
162 associated with hair follicles and other end organs and Aβ SA1-LTMRs found in both hairy and
163 glabrous skin also entrain to vibratory stimuli[2,52,56,57]. Therefore, it is likely that VPL neurons in
164 TrkB cKO and Ret cKO mice are sensitive to mechanical vibrations via inputs from primary
165 sensory neuron subtypes other than just Meissner and Pacinian corpuscle LTMRs[55,58]. In stark
166 contrast, vibration responsiveness of LCIC neurons was nearly absent in animals lacking
167 Pacinian corpuscles, although LCIC responses were normal in mice lacking Meissner corpuscles
168 (Fig. 2D, E, G). Taken together, these findings indicate that high frequency mechanical
169 vibrations acting on the body and detected by Pacinian corpuscle Aβ RA2-LTMRs are
170 prominently encoded in the LCIC.
171
172 **LCIC neurons integrate multimodal tactile-auditory stimuli in awake mice**
173 Recent recordings from Pacinian afferents under awake conditions revealed that Pacinian Aβ
174 RA2-LTMRs are exquisitely sensitive to environmental vibrations encountered during natural
175 behaviors[5]. Therefore, we next asked whether LCIC neurons are also sensitive to low amplitude
176 substrate vibrations in awake animals. We performed MEA recordings in awake head-fixed mice,
177 but instead of applying vibration directly to the paw, we vibrated the acrylic platform the animal
178 stood on (Fig. 3A). Remarkably, in awake mice, 100 percent of LCIC neurons with hindlimb
179 receptive fields responded robustly to 500 Hz stimulation of the surface platform, but few

responded to a 50 Hz stimulus, similar to results from direct stimulation of the limb in recordings from anesthetized mice (Fig. 1D, H, Extended Data Fig. 2G-H, Fig. 3B-C). Thus, as with Pacinian corpuscle Aβ RA2-LTMRs, LCIC neurons encode low-amplitude, high frequency environmental vibrations.

The inferior colliculus is primarily an auditory nucleus, and the LCIC receives extensive auditory input from brainstem auditory nuclei, prompting us to ask whether LCIC neurons responsive to high frequency tactile vibrations also respond to sound[1]. Prior findings indicate that many LCIC neurons are broadly tuned to auditory stimuli, and most auditory-sensitive LCIC neurons respond to short pulses of broadband noise[31,36,59,60]. Therefore, we exposed animals to 100 ms pulses of a broadband white noise stimulus (0-50 kHz) at a 65 dB sound pressure level (SPL) with the goal of activating LCIC neurons that receive auditory inputs. We delivered 500 Hz mechanical vibrations to the platform surface and white noise pulses in isolation, as well as coincident tactile-auditory stimulation (Fig. 3D) to awake mice while recording in the LCIC. Remarkably, ~75% of LCIC neurons were activated by both high frequency mechanical vibration of the platform and auditory white noise, with a minority of neurons responding to only platform vibration or sound (Fig. 3E, H). These findings reveal a high degree of convergence of auditory and mechanical vibration signals in the LCIC. Interestingly, of the LCIC neurons that received convergent tactile-auditory input, the majority had a larger response to coincident presentation of mechanical vibration and sound than to either vibration or sound alone (Fig. 3J, Extended Data Fig. 6D-I).

We further assessed the multimodal nature of LCIC responses to environmental vibrations by measuring responses of LCIC neurons in mice lacking either Pacinian corpuscles or cochlear function. As predicted from the findings in anesthetized mice (Fig. 2D-G), LCIC neurons in awake Ret cKO mice, which lack Pacinian corpuscles, were unresponsive to high frequency surface vibrations (Fig. 3F, I-J). Despite their insensitivity to vibration, LCIC neurons in Ret cKO mice were responsive to brush, suggesting that the LCIC receives inputs from other classes of cutaneous LTMRs (Extended Data Fig. 7D). It is noteworthy that deletion of Ret does not impact the auditory system, as the Auditory Brainstem Response (ABR) test in Ret cKO mice indicated similar auditory thresholds to littermate controls (Extended Data Fig. 7A-C).

211 Furthermore, LCIC neurons of Ret cKO mice were comparably sensitive to auditory white noise
212 stimuli compared to controls, indicating that developmental loss of Pacinian corpuscles does not
213 alter LCIC sensitivity to broadband auditory stimuli (Fig. 3F, I-J). In complementary
214 experiments, we tested whether disrupting auditory system function alters mechanical vibration
215 responsiveness in the LCIC. For this, we utilized *Sox10*^{Cre}*; Gjb2*$^{flox/flox}$ mice (Gjb2 cKO), which
216 lack connexin 26 expression in epithelial cells of the cochlea[61,62]. Gjb2 cKO mice lack cochlear
217 hair cell function but have an intact vestibular system, such that this congenital deafness model
218 exhibits extensive hearing loss but retains normal balance and motor function[61-65]. ABR testing in
219 Gjb2 cKO mice confirmed their inability to hear, as none of the Gjb2 cKO mice tested had a
220 discernable brainstem response at the highest sound level tested (Extended Data Fig. 8A-C).
221 Recordings in anesthetized Gjb2 cKO mice revealed that in the absence of normal hearing, LCIC
222 neurons exhibit robust responses to mechanical vibration stimulation (Extended Data Fig. 8F-G).
223 Force-frequency tuning curves in Gjb2 cKO showed no difference from controls (Fig S8F-G).
224 Furthermore, recordings in awake Gjb2 cKO mice demonstrated that LCIC neurons responded to
225 substrate vibrations although they showed no responsivity to white noise auditory stimuli (Fig.
226 3G, I-J). Thus, genetically disrupting either somatosensory/Pacinian corpuscle or auditory
227 system function does not grossly alter LCIC neuron responses to the other sensory modality.
228 These findings indicate that most LCIC neurons receive both auditory input emanating from the
229 cochlea and somatosensory input emanating from the body's Pacinian corpuscles. Therefore, the
230 LCIC is a site of auditory-mechanical vibration multisensory integration and enhancement (Fig.
231 3E-J, Extended Data Fig. 6).
232
233 **The LCIC mediates behavioral avoidance to tactile vibration**
234 The LCIC has been shown to mediate defensive behaviors in response to auditory cues[66]. To
235 begin investigating whether the LCIC can drive behavioral responses to high frequency
236 mechanical vibrations, we developed a behavioral preference assay that relies on an animal's
237 ability to detect and respond to high frequency mechanical vibrations of the environment.
238 Animals were placed in a two-chamber behavioral setup where the floor of one chamber vibrates
239 at 500 Hz, a stimulus that robustly activates Pacinian corpuscle afferents and the LCIC of awake
240 animals (Fig. 3B, E., Fig. 4A, Fig. S9A-D)[5]. Wildtype animals had a strong and reliable
241 preference for the non-vibrating chamber, spending ~80% of their time there when the vibration

242 stimulus was on (Fig. 4B-C, Extended Data Fig. 9E-H). Since the production of the 500 Hz
243 vibration generated a low amplitude 500 Hz auditory tone, we performed a sound-only control.
244 We decoupled the vibration motor from the chamber floor, such that a comparable sound was
245 produced with no surface vibration. In the sound-only paradigm, animals showed no aversion
246 toward the stimulus side of the chamber, demonstrating that sound alone does not drive a
247 preference (Fig. 4D). To test whether the behavior is dependent on Pacinian corpuscles, the
248 behavioral preference assay was done using Ret cKO mice, which lack Pacinian corpuscles. Ret
249 cKO mice demonstrated no preference for the non-vibrating side of the chamber over the
250 vibrating side, indicating that avoidance of the 500 Hz vibration stimulus is dependent on
251 Pacinian corpuscles (Fig. 4E-F, Extended Data Fig. 9I-J).
252
253 The vibration place preference assay was next used to determine whether avoidance of 500 Hz
254 mechanical vibration is dependent on the LCIC. Targeted, bilateral injections of a fluorescently-
255 tagged GABA-A receptor agonist, muscimol, were used to silence neural activity in the inferior
256 colliculus (IC) (Fig. 4G, Extended Data Fig. 10C). Post-hoc histology confirmed that muscimol
257 was reliably restricted to the IC and did not extend into neighboring brain regions, including the
258 superior colliculus, periaqueductal gray, or cerebellum (Fig. 4G, Extended Data Fig. 10A-B)[66-68].
259 IC-silenced mice displayed normal locomotor activity, traveling equal distances during the assay
260 as controls (Fig. 4H). Strikingly, IC-silenced mice did not exhibit avoidance of the vibratory
261 stimulus compared to saline injected controls, revealing that the IC is required for the behavioral
262 response to high frequency mechanical vibration (Fig. 4I-K, Extended Data Fig. 10D). To
263 determine whether the IC is required for general behavioral avoidance, or whether the effect of
264 IC silencing is specific to vibratory stimuli, we also tested whether IC silencing alters avoidance
265 of other somatosensory stimuli. We first performed a texture preference assay in saline and
266 muscimol treated mice. In a two-chamber setup, one side of the chamber was covered in a
267 smooth construction paper, while the other side was covered with a coarse grit sandpaper, which
268 is aversive (Fig. 4L, Extended Data Fig. 10F-G). Mice injected with either saline or muscimol in
269 the IC showed strong preference for the smooth side of the chamber, revealing that the IC is not
270 necessary for aversive texture avoidance (Fig. 4M). A cold temperature avoidance test was also
271 performed. For this, we used a two-chamber cold avoidance assay in which mice were given a
272 choice between one chamber, which was held at room temperature (30 ^{o}C), and a second

273 chamber, which was held at 18 °C (Fig. 4N, Extended Data Fig. 10E). Similar to the texture
274 preference assay, both control and IC-silenced animals displayed robust avoidance of the cold
275 chamber (Fig. 4O). These findings indicate that the IC mediates behavioral response to high
276 frequency mechanical vibrations but is not required for avoidance of an aversive texture or
277 temperature.
278
279 **Discussion**
280 The majority of research into the neurobiological basis of discriminative touch of the body has
281 focused on the ascending pathway through the thalamus (VPL) to somatosensory cortex (S1),
282 while somatosensory representations in other brain areas have remained largely unexplored.
283 Here, we report that neurons in the LCIC and VPL exhibit highly distinct vibrotactile tuning
284 properties that may underlie unique functions of divergent ascending somatosensory system
285 streams. Most VPL neurons had restrictive receptive fields and were tuned to low frequency
286 vibrations. These properties are well suited for tactile acuity and discrimination—functions
287 hypothesized to be mediated by the VPL to S1 pathway[69-72]. Only a small fraction of VPL
288 neurons (~9%) encoded high frequency vibration (Fig. 1H). In contrast, most LCIC neurons
289 exhibited expansive receptive fields and were tuned to high frequency vibrations (>75%)
290 conveyed by Pacinian corpuscle Aβ RA2-LTMRs (Fig. 1H). The salience of low amplitude
291 environmental vibrations encoded in the LCIC is highlighted by our finding that IC silencing
292 virtually eliminated animals' avoidance of a 500 Hz vibratory stimulus in a place preference
293 paradigm (Fig. 4I-J, Extended Data Fig. 10D). It is possible that the divergent ascending streams
294 through the LCIC and VPL underlie distinct responses to high frequency vibrations in different
295 contexts. For example, the sparser representation of high frequency vibration in the VPL to S1
296 stream may underlie operant tasks that use vibratory cues[16,71-73]. Future work will discern the
297 relative contributions of distinct ascending streams encoding environmental vibrations in
298 different contexts.
299
300 Strikingly, most mechanical vibration sensitive LCIC neurons are also tuned to auditory stimuli.
301 Moreover, the majority of LCIC neurons that received convergent mechanical vibration and
302 auditory inputs exhibited multisensory enhancement, responding more strongly to coincident
303 tactile-auditory stimulation than to either modality alone (Fig. 3H-J. Extended Data Fig. 6E-F).

Thus, the LCIC encodes environmental vibrations, whether they are mechanical vibrations propagated through the ground, detected by Pacinian corpuscles, and conveyed via the ascending somatosensory pathway or sound waves traveling through air, captured by the cochlea, and conveyed via the ascending auditory pathway (Extended Data Fig. 10H). We suspect that the LCIC enables enhanced detection or reaction to environmental cues through auditory and vibrotactile coincidence detection. A myriad of natural phenomena generates coincident sounds and substrate vibrations, including wind, rivers, seismic events or earth movements, objects moving across or falling to the ground, vocalizations or rumblings of conspecifics, and the motions of prey or predators. Multisensory audio-vibrotactile integration in the LCIC may increase saliency of these ethologically relevant environmental cues and may be particularly instrumental under conditions in which cues are weak and difficult to discern. We propose that, through their convergent inputs to the LCIC, the somatosensory and auditory systems collaborate to detect, localize, and respond to environmental vibrations.

Figures and Legends

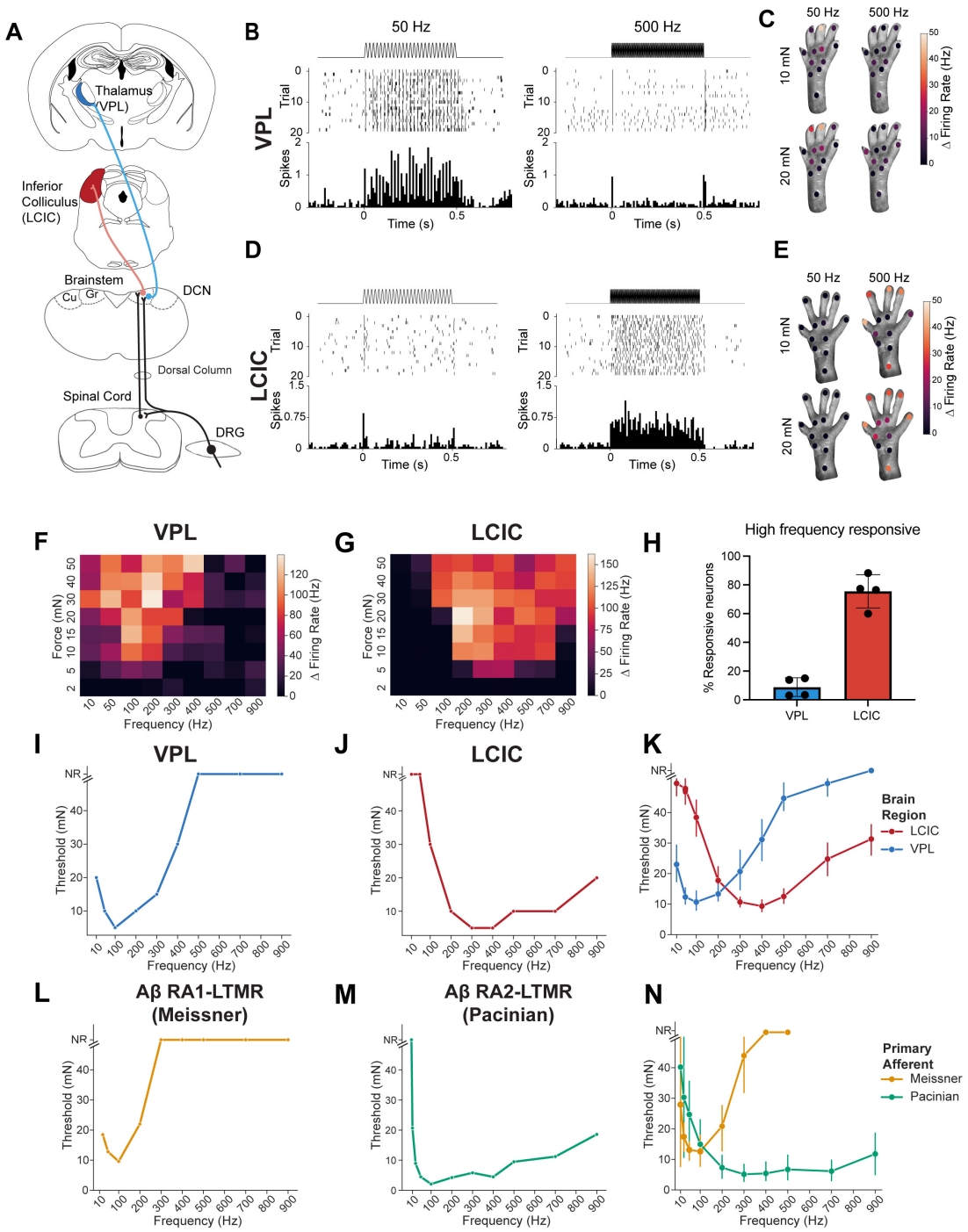

Figure 1: LCIC and VPL neurons are differentially tuned to mechanical vibratory stimuli. **A)** The brainstem dorsal column nuclei (DCN) receive inputs from dorsal root ganglia (DRG) primary sensory neurons and spinal cord projection neurons. Non-overlapping subsets of DCN

projection neurons target the ventroposterolateral thalamus (VPL; blue) and the external nucleus of the inferior colliculus (LCIC; red).

B and D) Representative VPL (B) and LCIC (D) neuron spike raster and histogram in response to 50 Hz and 500 Hz vibratory stimuli delivered at a 10 mN force to the hindlimb. Top: spike raster; bottom: average histogram in 10 ms bins.

C and E) Example VPL (C) and LCIC (E) neuron receptive field organization for 50 Hz and 500 Hz stimulation to multiple regions across the hindlimb, delivered at 10 mN and 20 mN intensities. Stimulus locations are superimposed on images of the hindpaw.

F and G) Representative VPL (F) and LCIC (G) neuron responses to vibrational frequencies delivered at different forces to the hindlimb. Heatmap intensity corresponds to the neuron's average change in firing to the sustained portion of vibratory stimuli (200 ms window beginning 50 ms after stimulus onset).

H) Percentage of neurons (mean ± SD) with hindbody brush receptive fields (tested by brushing the hindpaw, thigh, and trunk) that respond to 500 Hz stimulation of the limb at a 10 mN force in the VPL (n= 182 neurons from 4 animals) and LCIC (n= 76 neurons from 4 animals). Each data point corresponds to measurements in one animal. See also Extended Data Fig. 3.

I and J) Force-frequency threshold curves obtained from heatmaps in F and G, where the force threshold for a vibrational frequency is defined as the minimum force required to elicit 20% of the neuron's maximum firing during the sustained portion of the stimulus. Frequencies in which the highest force tested (50 mN) failed to reach threshold are designated NR (non-responsive).

K) Average threshold curves (mean ± 95% confidence interval) for neurons responsive to hindlimb vibration recorded in the VPL (n=15 neurons from 6 animals) and LCIC (n=22 neurons from 6 animals).

L and M) Force-frequency threshold curves for representative Meissner corpuscle innervating Aβ RA1-LTMR afferent (L) and Pacinian corpuscle innervating Aβ RA2-LTMR afferent (M). Threshold is defined as the minimum force necessary for the neuron to reach 50% vibratory entrainment. Frequencies in which the highest force tested (50 mN) failed to reach threshold are designated NR (non-responsive).

N) Average threshold curves (mean ± 95% confidence interval) for hindlimb Meissner Aβ RA1-LTMRs (n=4 neurons from 4 animals) and Pacinian Aβ RA2-LMTRs (n=6 neurons from 5 animals).

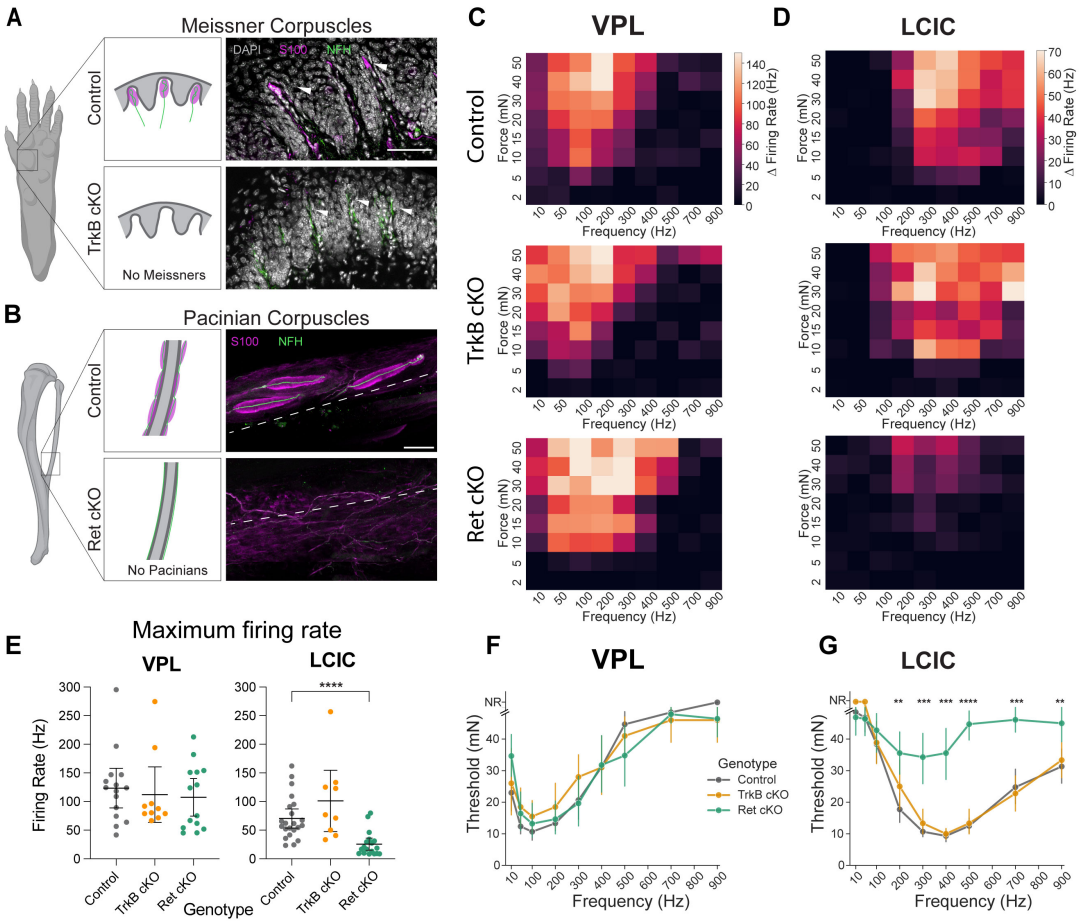

Figure 2: LCIC vibration responses are mediated by Pacinian corpuscle Aβ RA2-LTMRs. **A)** Meissner corpuscles, located in the plantar pad and digit glabrous skin, are absent in *Avil*^{Cre}; *TrkB*$^{flox/flox}$ (TrkB cKO) mice, which lack TrkB in DRG sensory neurons. Images of skin histology from a TrkB cKO and littermate control, stained for anti-NFH (labels myelinated axons, green) and anti-S100 (labels glial cells, magenta). Scale bar = 50 µm. See also Extended Data Fig. 4 for quantification.

B) Pacinian corpuscles, located in the periosteum of the fibula, are absent in *Avil*^{Cre}; *Ret*$^{flox/flox}$ (Ret cKO) mice, which lack Ret in DRG sensory neurons. Images of whole mount histology of the limb of a Ret cKO animal and littermate control, stained for anti-NFH and anti-S100 to visualize Pacinian corpuscles. White dashed line indicates position of the fibula. Scale bar = 100 µm. See Extended Data Fig. 4 for quantification.

C and D) Force-frequency heat maps for representative VPL (C) and LCIC (D) neurons in control, TrkB cKO and Ret cKO animals. Heatmap intensity corresponds to the neuron's average change in firing to the sustained portion of vibratory stimuli.

E) Maximum firing rate for VPL and LCIC (mean ± 95% confidence interval) neurons to vibratory stimuli in control, TrkB cKO and Ret cKO mice. Firing rates of LCIC neurons in Ret cKO and control mice were significantly different (****$p<0.0001$ Mann-Whitney U test). Firing rates of VPL neurons in TrkB cKO, Ret cKO, and controls were not significantly different. Firing rates of LCIC neurons in TrkB cKO and controls were not significantly different (Mann-Whitney U test).

F) Average threshold curves of VPL neurons (mean ± 95% confidence interval) recorded in control (n=15 neurons from 6 animals), TrkB cKO (n=10 neurons from 3 animals), and Ret cKO (n=14 neurons from 4 animals) mice. Thresholds between Ret cKO, TrkB cKO and controls were not significantly different (Mann-Whitney U Test with Bonferroni correction for multiple comparisons).

G) Average threshold curves of LCIC neurons (mean ± 95% confidence interval) recorded in control (n=22 neurons from 6 animals), TrkB cKO (n=9 neurons from 4 animals), and Ret cKO (n=18 neurons from 4 animals) mice. (*$p<0.05$, **$p<0.01$, ***$p<0.001$, ****$p<0.0001$, Mann-Whitney U test with Bonferroni correction for multiple comparisons). While thresholds between Ret cKO and controls were significantly different, thresholds between TrkB cKO and controls were not (Mann-Whitney U Test with Bonferroni correction for multiple comparisons).

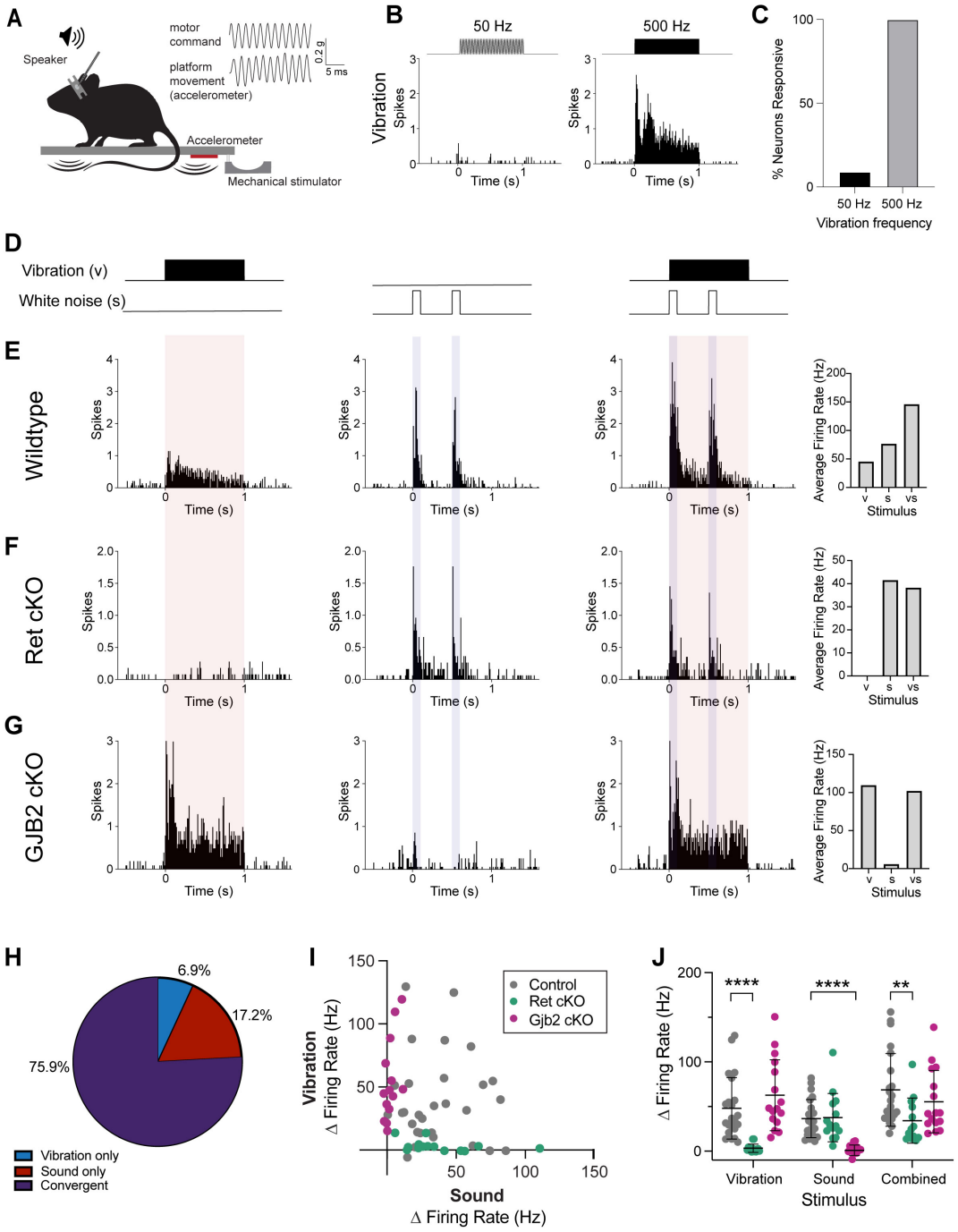

Figure 3: Audio-tactile multimodality of LCIC neurons in awake mice.

A) Recordings of LCIC neurons were conducted in awake head-fixed mice as they stood on an acrylic platform, which could be stimulated at different vibratory frequencies. An accelerometer was attached underneath the acrylic platform to measure vibration frequency and amplitude. An

example motor command and accelerometer signal are shown for 500 Hz vibration of the platform. A speaker is positioned on the contralateral side of the head from the recording site.

B) Peristimulus time histogram (PSTH) for a representative LCIC neuron, aligned to 50 Hz (left) and 500 Hz (right) vibration stimulation of the acrylic platform at a vibration amplitude of ~0.2 g (gravitational acceleration). PSTHs are baseline subtracted and reported in 10 ms bins.

C) Percentage of hindlimb sensitive LCIC neurons that responded to 50 Hz and 500 Hz vibratory stimuli (n=24 neurons from 5 animals).

D) 500 Hz substrate vibration (amplitude 0.2 g) and auditory white noise (frequency 0-50 kHz, 100 ms pulses, 65 dB SPL) were delivered in isolation and coincidentally to awake head-fixed mice.

E) Example PSTHs from an LCIC neuron of a wildtype mouse aligned to vibration (v), sound (s) and convergent (vs) stimuli. PSTHs are baseline subtracted and in 10 ms bins. Right: The example neuron's average firing (during 0-0.1 s and 0.5-0.6 s windows) for each stimulus type.

F and G) As in (E), example LCIC neurons in a Ret cKO animal, which lacks Pacinian corpuscles (F), and a Gjb2 cKO animal, which is unable to hear (G).

H) Percentage of neurons in control animals that respond to 500 Hz vibration only, sound only, or convergent stimuli (n=29 neurons from 5 animals).

I) Scatter plot of each neuron's average change in firing rate to vibration and sound stimuli in control (n=29 neurons from 5 animals), Ret cKO (n=14 neurons from 3 animals) and Gjb2 cKO (n=15 neurons from 3 mice) animals.

J) Average change in firing rate to vibration, sound, or combined stimuli (mean ± SD) in control (n=29 neurons from 5 animals), Ret cKO (n=14 neurons from 3 animals) and Gjb2 cKO (n=15 neurons from 3 mice) animals (**$p<.01$, ***$p<0.001$, ****$p<0.0001$, Mann-Whitney U test).

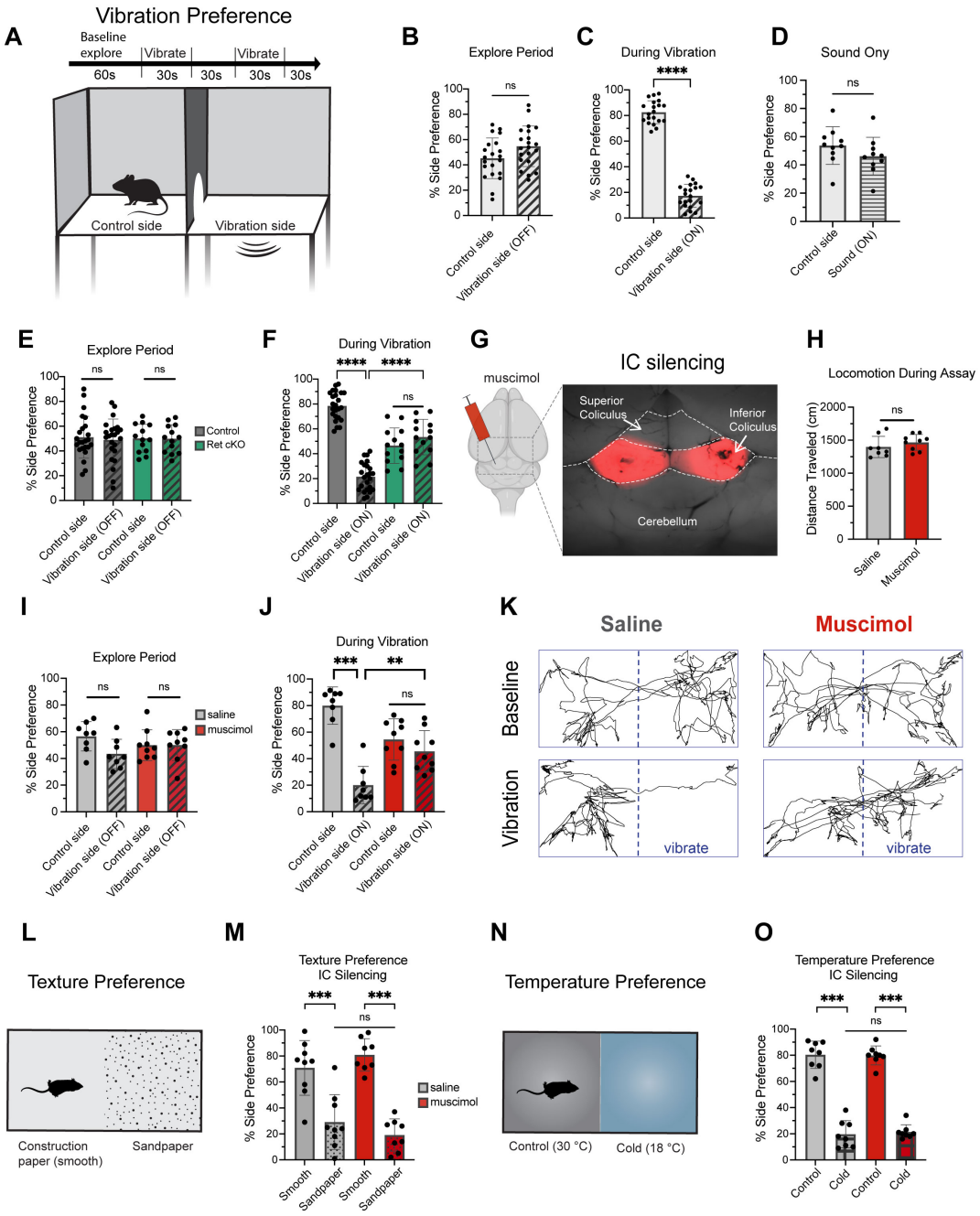

Figure 4: The LCIC mediates behavioral avoidance to platform vibration.

A) Animals were placed in a 2-chamber behavioral setup. The floors of each chamber are disconnected to prevent propagation of vibration between them, and an exciter speaker is attached to the floor of one chamber to generate mechanical vibrations. The chamber walls are partially open to prevent sound resonance from the exciter.

B and C) The percentage of time wildtype CD-1 animals spend on each side of the chamber (mean ± SD) during the 60 s baseline explore period (B) and the vibration periods (C) of the trial. Each dot represents one animal (n=20 animals, ****p<0.0001 paired t-test).

D) The speaker was detached from the floor of the chamber to test whether the sound of the exciter speaker alone can drive a behavioral preference. Time spent on each side of the chamber during the sound on periods was not statistically different (n=10 animals, paired t-test).

E and F) The percentage of time Ret cKO mice (n=14 animals) and littermate controls (n=24 animals) spent on each side of the chamber during the 60 s baseline explore period (E) and the vibration periods (F) of the behavioral trial. (****p<0.0001, paired t-test within group, unpaired t-test between groups).

G) Targeted injections of TMR-X conjugated to the GABA-A receptor agonist, muscimol, were used to silence neural activity in the inferior colliculus. Top-down view of a schematic (left) and representative muscimol injected brain. Dotted lines depict borders between the inferior colliculus and indicated neighboring brain regions.

H) Total distance traveled during the behavioral assay in saline injected controls (n=8) and muscimol injected animals (n=9 animals, not significant, unpaired t-test).

I and J) The proportion of time muscimol injected mice (n=9 animals) and saline injected controls (n=8 animals) spent on each side of the chamber during the 60 s baseline explore period (I) and the vibration periods (J) of the trial. (**p<0.01, ***p<0.001, paired t-test within group, unpaired t-test between groups)

K) Representative activity traces for saline injected (control) and muscimol injected animals during the baseline and vibration periods of the behavioral trial. See also Extended Data Fig. 9.

L) Schematic of texture preference assay.

M) Percentage of time spent on the smooth and rough sides of the chamber during the 10 min assay for saline controls (n=9 animals) and muscimol silenced animals (n=9 animals, ***p<0.001, paired t-test within group, unpaired t-test between groups).

N) Schematic of temperature preference assay.

O) Percentage of time spent on the control (30 °C) and cold (1 8°C) sides of the chamber during the 5 min assay for saline controls (n=8) and muscimol silenced animals (n=8, ***p<0.001, paired t-test within group, unpaired t-test between groups).

Extended Data Figures and Legends

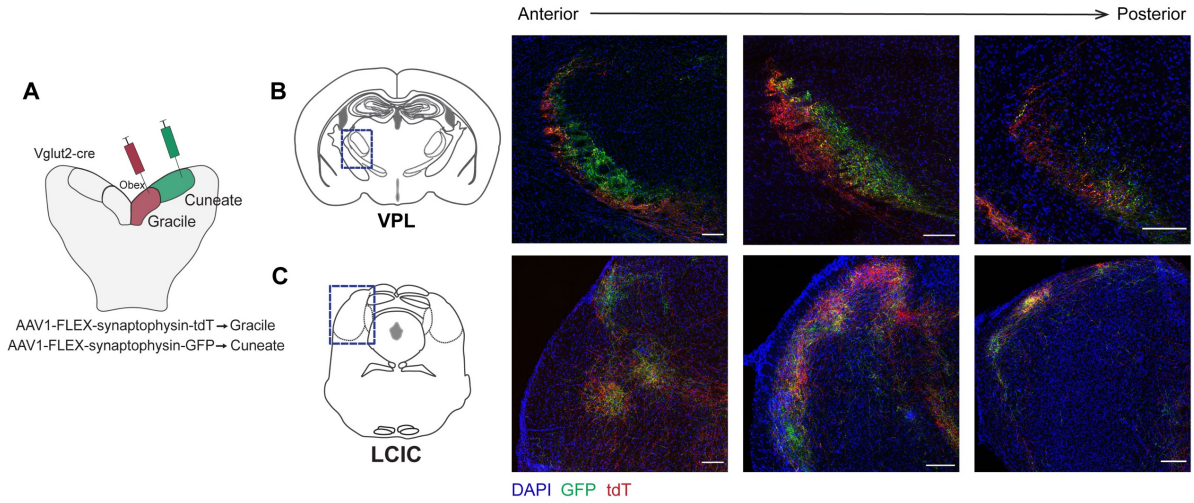

Extended Data Figure 1: Anterograde tracing from the dorsal column nuclei.

A) To identify downstream projections from the dorsal column nuclei (DCN), an AAV encoding Cre-dependent synaptophysin-tdT was injected into the gracile nucleus and an AAV encoding Cre-dependent synaptophysin-GFP was injected into the cuneate nucleus of Vglut2-Cre mice. **B-C)** TdT and GFP positive terminals were observed throughout the ventroposterolateral thalamus (VPL) and lateral cortex of the inferior colliculus (LCIC). Scale bar = 150μm.

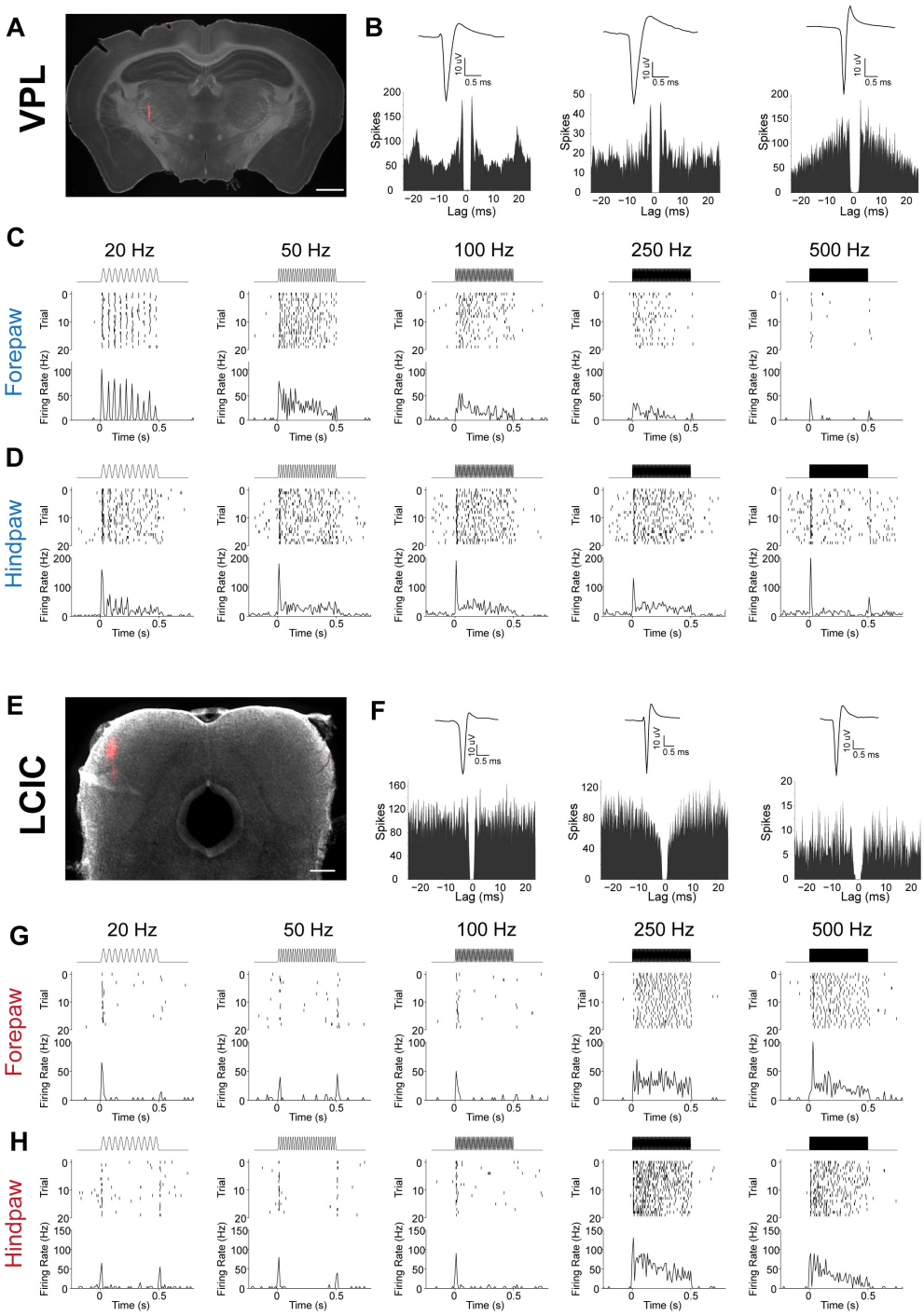

Extended Data Figure 2: MEA recordings in the VPL and LCIC to characterize vibratory responses.

A) Representative probe tract from MEA recording in the VPL. Scale bar = 1000µm.

B) Average waveforms and corresponding autocorrelogram for three example VPL neurons.

C) Example VPL neuron raster and PSTHs in response to vibration of different frequencies delivered at a 10 mN force to the forelimb. Top: spike raster; bottom: PSTHs, which are baseline subtracted and in 10ms bins.

D) Same as C for a hindlimb responsive neuron.

E) Representative probe tract from MEA recording in the LCIC. Scale bar = 500 μm.

F) Average waveforms and corresponding autocorrelogram for three example LCIC neurons.

G) Same as C for an example LCIC neuron.

H) Same as D for an example LCIC neuron.

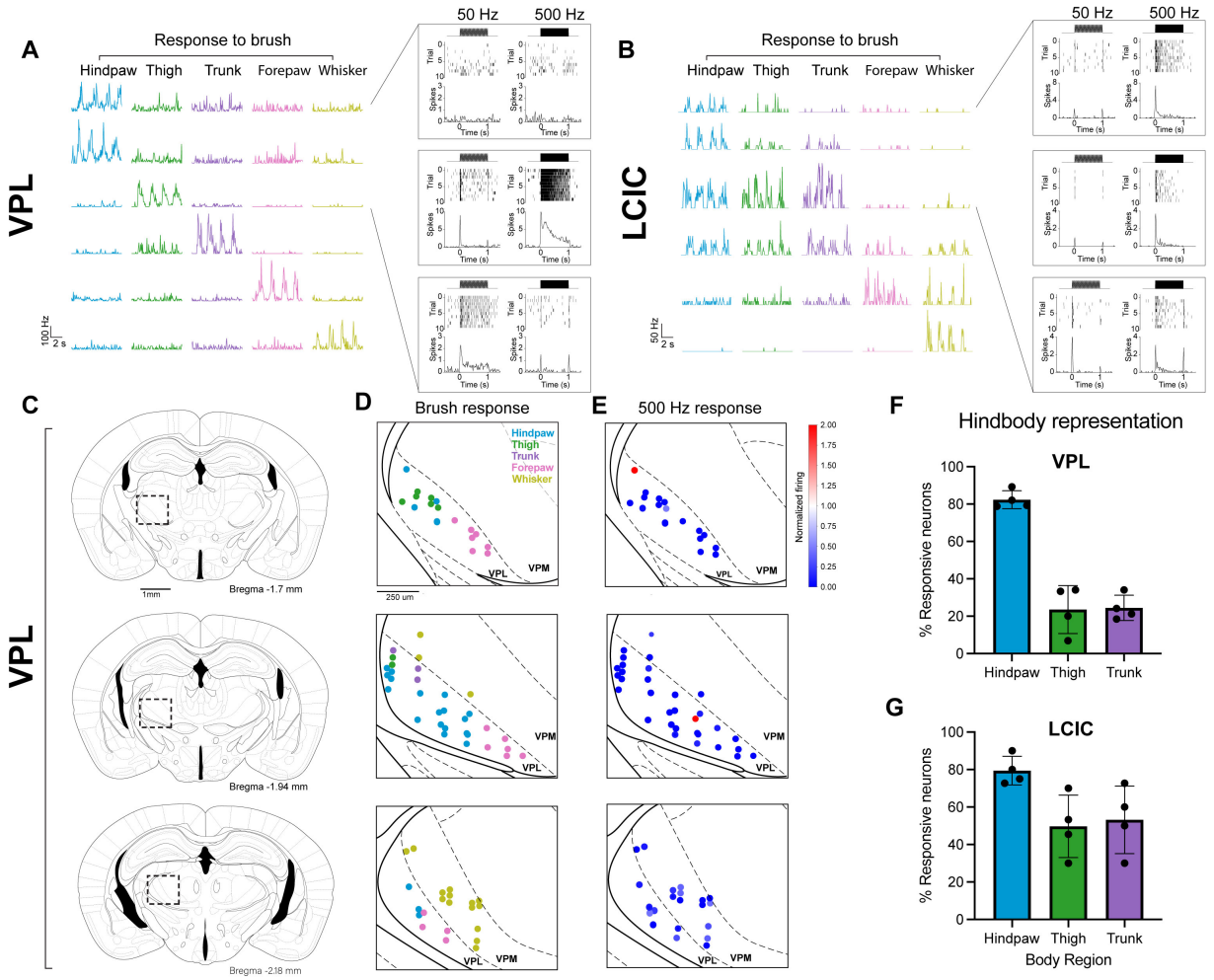

Extended Data Figure 3: Somatotopic and vibratory mapping in the VPL and LCIC.

A) Representative VPL neurons responding to brush of different regions of the body. Each row corresponds to one neuron. Each body region is stroked four times per trial. Right: Example raster plot and PSTHs aligned to hindlimb vibration at 50 Hz and 500 Hz at 10 mN, corresponding to adjacent brush responsive neurons. PSTHs are baseline subtracted and in 10ms bins.

B) As in A, representative LCIC neurons. Note that, unlike VPL neurons, most LCIC neurons respond to brush across multiple body locations.

C-E) Example mapping of the VPL in one animal, shown at different coronal planes on the anterior-posterior axis. The approximate atlas location (C) for recorded neurons is shown for the corresponding somatotopic map of the VPL (D), where each neuron is colored for the body region most responsive to brush. The same neurons shown in D are colored by their

485 responsiveness to 500 Hz mechanical vibration, which is normalized to the neuron's response to
486 brush (E). Note that most brush responsive VPL neurons do not respond to the 500 Hz vibration
487 stimulus during the sustained period of the stimulation.
488 **F and G)** Percentage of neurons (mean ± SD) with hindbody receptive fields that respond to
489 brush of the hindpaw, thigh, and trunk in the VPL (F) (n= 182 neurons from 4 animals) and LCIC
490 (G) (n= 76 neurons from 4 animals). Each data point corresponds to a single animal.

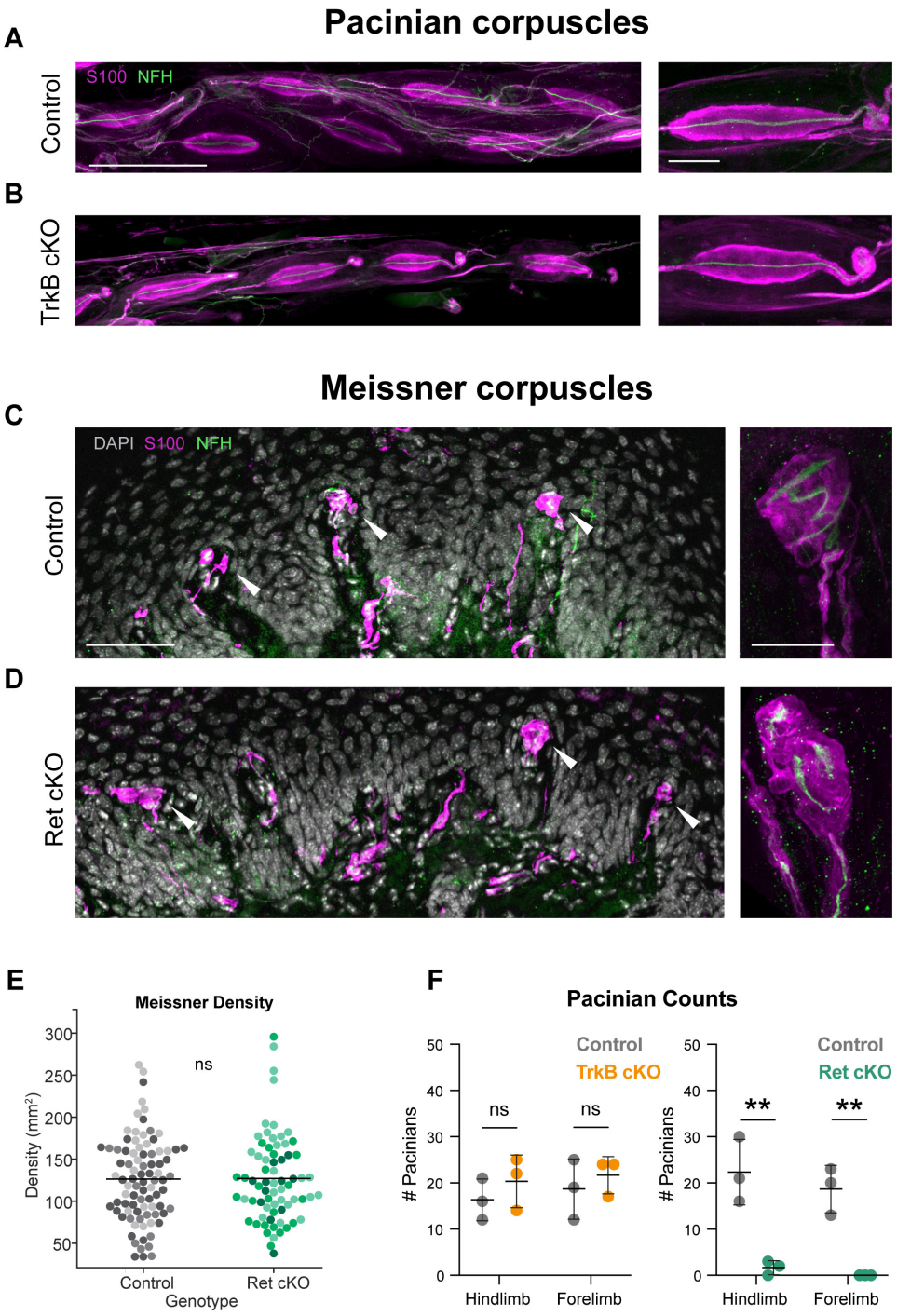

Extended Data Figure 4: Anatomical characterization of peripheral endings in Ret cKO and TrkB cKO mice.

A-B) Images of Pacinian corpuscles from the limbs of TrkB cKO animals and littermate controls. Limbs were whole-mount stained with antibodies against NFH (green), which labels large caliber

496 axons, and S100 (magenta), which labels lamellar cells of the corpuscle and myelinating
497 Schwann cells. Left scale bar = 250μm. Right scale bar = 50 μm.
498 **C-D)** Images of Meissner corpuscles (indicated by white arrows) from Ret cKO animals and
499 littermate controls. Skin tissue was stained using antibodies against NFH (green) and S100
500 (magenta). DAPI staining is shown in gray. Left scale bar = 50 μm. Right scale bar =20 μm.
501 **E)** Quantification of Meissner density in Ret cKO (n=3 animals) and littermate controls (n=3
502 animals). Each data point is the Meissner density for a single skin section, and data points of the
503 same color came from the same animal (no significant difference using unpaired t-test).
504 **F)** Quantification of Pacinian corpuscles in TrkB cKO (n=3 animals) and littermate controls (n=3
505 animals), and Ret cKO (n=3 animals) and littermate controls (n=3 animals). The number of
506 Pacinians was counted from wholemount staining of hindlimbs and forelimbs (mean ± SD,
507 **$p<0.001$, unpaired t-test).

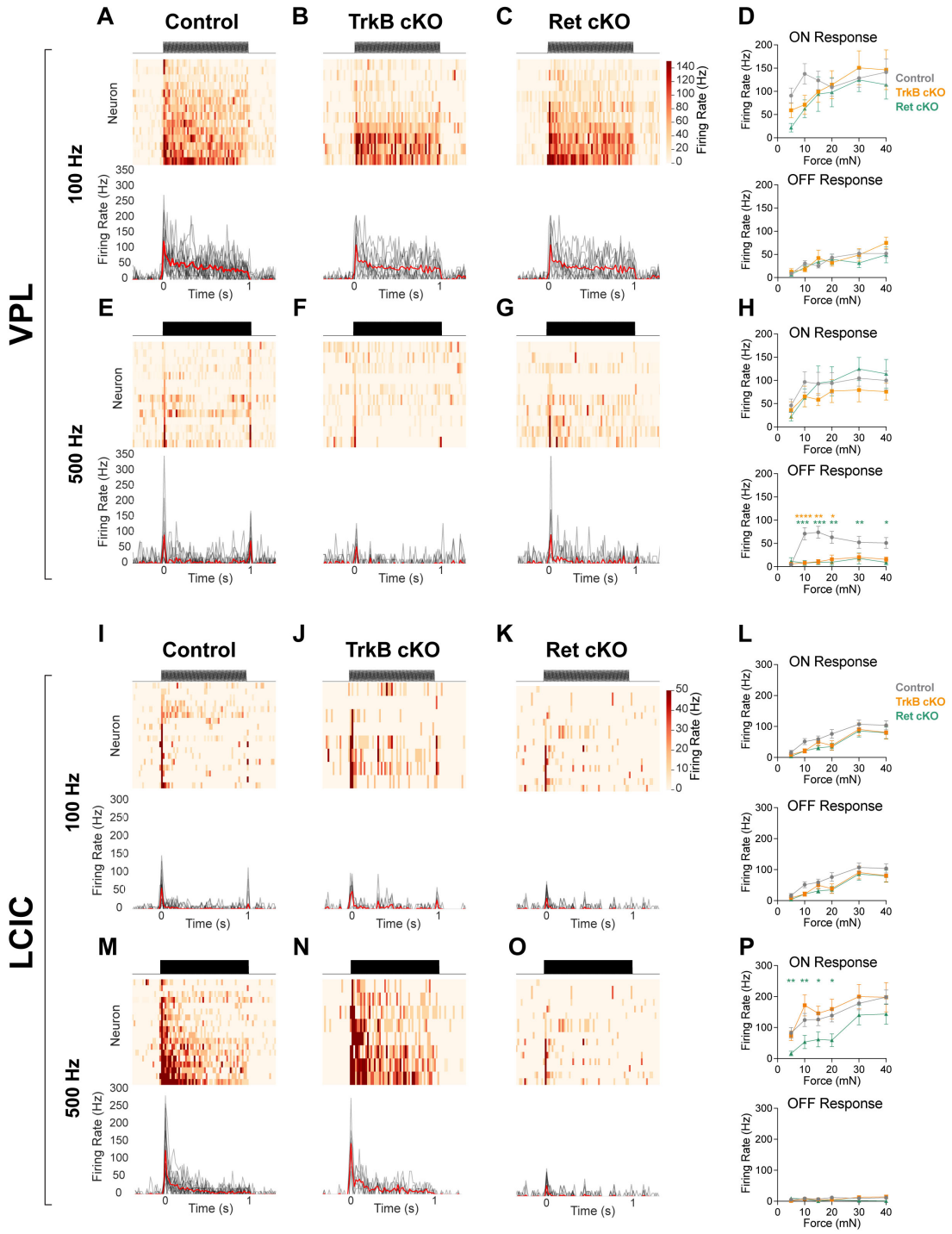

508

509 **Extended Data Figure 5: Onset and offset responses to vibratory stimuli in Ret cKO and**

510 **TrkB cKO mice.**

511 **A)** Top: Heatmap of neurons in the VPL responding to 100 Hz vibration at a 15 mN force (n=14

512 neurons from 6 animals). Each row is one neuron. Bottom: PSTHs of each neuron in above

513 heatmap (gray), and population average PSTH (red). PSTHs are in 20ms bins.

B-C) Same as A in TrkB cKO (n=10 neurons from 3 animals) and Ret cKO mice (n=14 neurons from 4 animals).

D) Average firing rate of VPL neurons to the onset (top) and offset (bottom) of the 100 Hz vibration stimulus in control, TrkB cKO, and Ret cKO mice (mean ± SEM, not significantly different, Mann-Whitney U test with Bonferroni correction for multiple comparisons). On period is 20 ms after the stimulus onset, and off period is 20 ms after the end of the stimulus.

E-G) Same as A-C to 500 Hz vibration at 15 mN.

H) Same as D for 500 Hz stimulus (*$p<0.05$, **$p<0.01$, ***$p<0.001$, ****$p<0.0001$, Mann-Whitney U test with Bonferroni correction for multiple comparisons).

I-K) Same as A-C for neurons in the LCIC in control (n=18 neurons from 5 animals), TrkB cKO (n=8 neurons from 4 animals), and Ret cKO (n=16 neurons from 5 animals) animals.

L) Average firing rate of LCIC neurons to the onset (top) and offset (bottom) of the 100 Hz vibration stimulus in control, TrkB cKO, and Ret cKO mice (mean ± SEM, not significantly different, Mann-Whitney U test with Bonferroni correction for multiple comparisons).

M-O) Same as I-K to 500 Hz vibration at 15 mN.

P) Same as L for a 500 Hz stimulus (*$p<0.05$, **$p<0.01$, Mann-Whitney U test with Bonferroni correction for multiple comparisons).

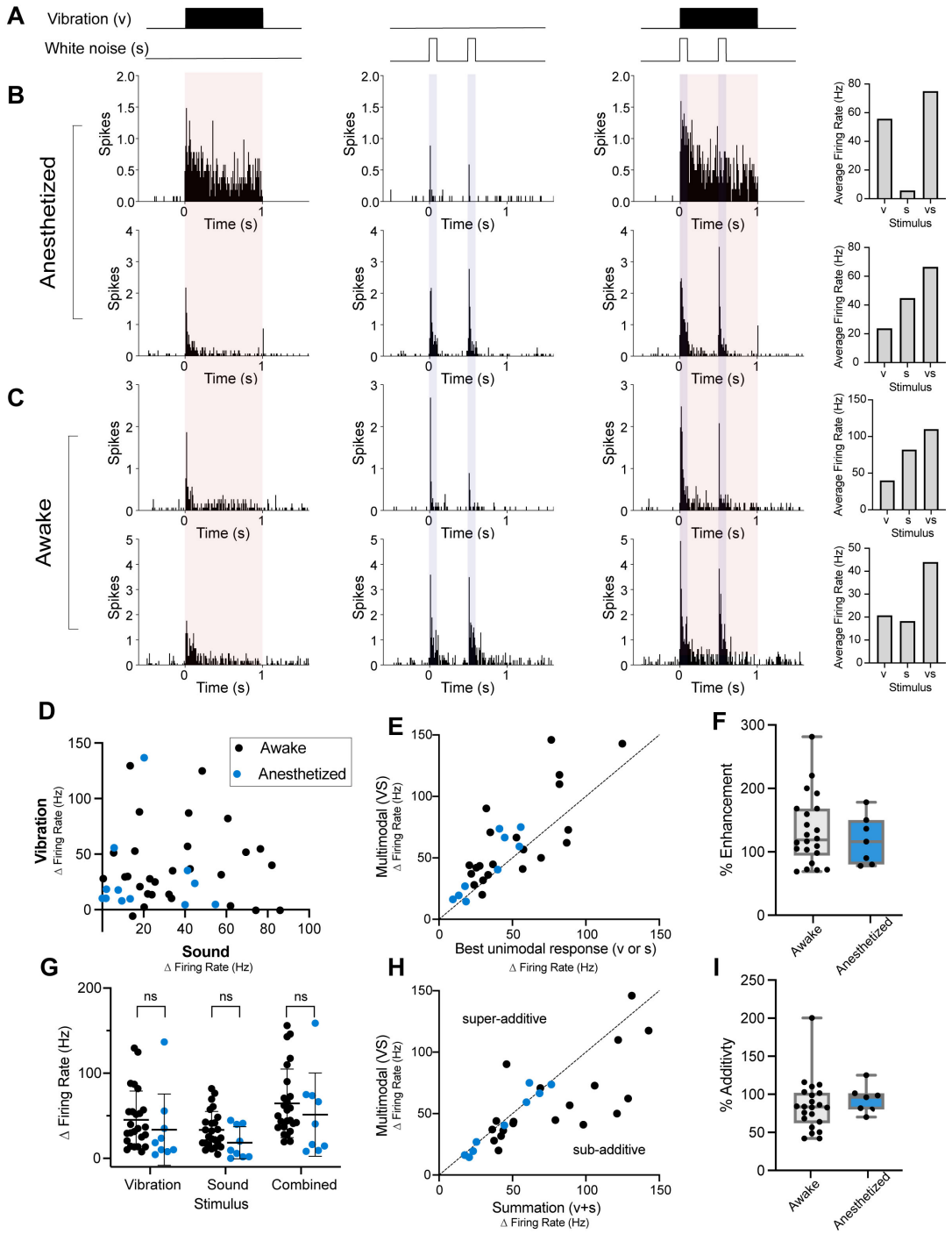

Extended Data Figure 6: Audio-tactile multimodality of LCIC neurons in awake and anesthetized animals.

A) 500 Hz substrate vibration and auditory white noise (frequency 0-50 kHz, 100 ms pulses, 65 dB SPL) were delivered in isolation and coincidentally, as in Fig. 3.

536 **B)** Example PSTHs from two wildtype neurons aligned to vibration (v), sound (s) and
537 convergent (vs) stimuli in anesthetized animals. PSTHs are baseline subtracted and in 10ms bins.
538 Right: The example neuron's average firing (during 0-0.1 s and 0.5-0.6 s windows) for each
539 stimulus type.
540 **C)** Same as B, except recordings were done in awake animals.
541 **D)** Scatter plot of change in firing rate to vibration or sound in neurons from awake (n=29
542 neurons from 5 animals) and anesthetized mice (n=9 neurons from 3 animals).
543 **E)** Scatter plot of firing rates in response to combined vibration and sound (vs) plotted against
544 best unimodal response (vibration only or sound only). Unitary line denotes equal firing between
545 best unimodal stimulus and combined stimulus conditions.
546 **F)** Quantification of multisensory enhancement in awake and anesthetized conditions
547 (corresponding to E), calculated using the following equation: $\frac{\mathrm{vs}-(\mathrm{Max(v\ or\ s)})}{\mathrm{Max(vor\ s)}}*100$. Neurons
548 above 100% display multisensory enhancement[74,75].
549 **G)** Average change in firing rate to vibration, sound, or combined stimuli (mean ± SD) in control
550 (n=29 neurons from 5 animals), and anesthetized (n=9 neurons from 3 animals) conditions (not
551 significant, Mann-Whitney U test).
552 **H)** Scatter plot of firing rates in response to combined vibration and sound (vs) plotted against
553 hypothetical summed vibration and sound responses (v+s). Unitary line denotes equal firing to
554 combined stimulation (vs) and the sum of firing to vibration and sound stimuli (v+s).
555 **I)** Quantification of multisensory integration in awake and anesthetized conditions
556 (corresponding to H), calculated using the following equation: $\frac{\mathrm{vs}-(\mathrm{v+s})}{\mathrm{v+s}}*100$. Neurons above
557 100% display super-additivity and neurons below 100% display sub-additivity[75,76].

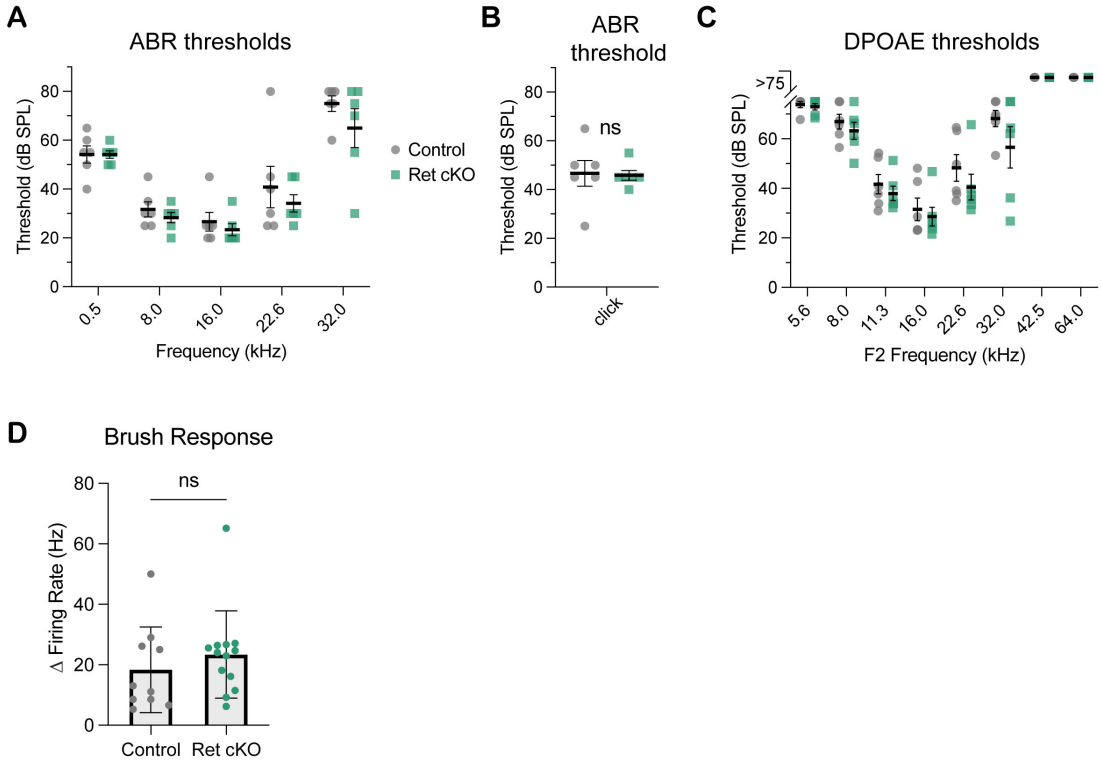

Extended Data Figure 7: Ret cKO mice have normal auditory thresholds and brush responses.

A) Auditory brainstem response (ABR) thresholds were measured in Ret cKO mice and littermate controls at 5 different auditory frequencies (mean ± SEM). Auditory thresholds between Ret cKO (n=6 animals) and controls (n=6 animals) were not significantly different (Mann-Whitney U Test with Bonferroni correction for multiple comparisons).

B) ABR thresholds to a broadband frequency "click" were measured in Ret cKO mice (n=6 animals) and littermate controls (n=6 animals). Thresholds were not significantly different (Mann-Whitney U Test).

C) Distortion product otoacoustic emissions (DPOAE) thresholds, which are sounds generated by mechanically active cells in the ear in response to sound stimuli, were measured in Ret cKO mice (n=6 animals) and littermate controls (n=6 animals) for 8 different frequency pairs (mean ± SEM). Thresholds were not significantly different (Mann-Whitney U Test with Bonferroni correction for multiple comparisons), suggesting normal function of the sensory cells responsible for fine-tuning cochlear gain.

574 **D)** Average change in firing to brush stimuli applied to the hindbody of LCIC neurons in awake
575 control (n=10 neurons) and Ret cKO (n=13 neurons) mice. Responses to brush were not
576 significantly different (Mann-Whitney U Test).

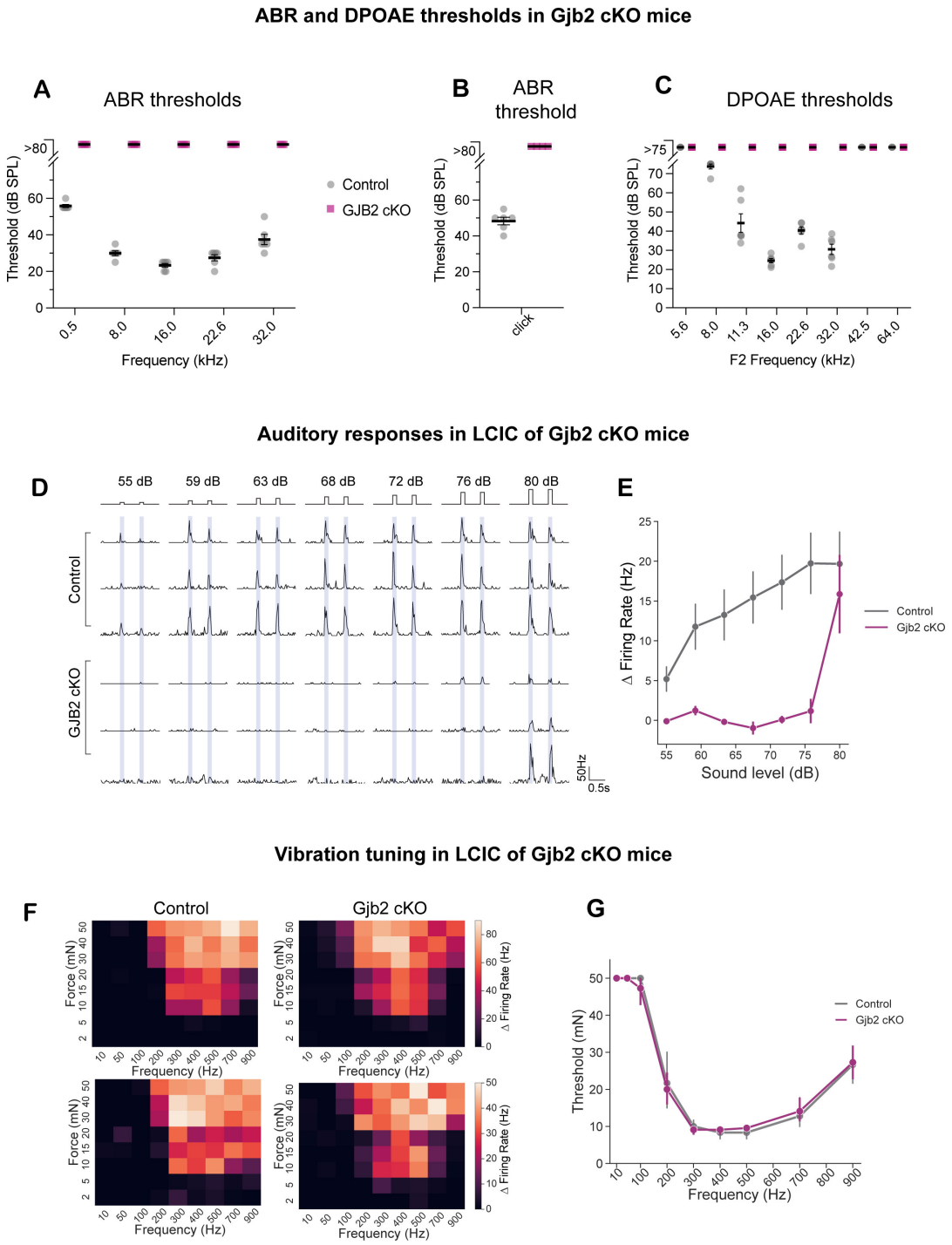

Extended Data Figure 8: Characterization of auditory and tactile responses in anesthetized Gjb2 cKO mice.

A) Auditory brainstem response (ABR) thresholds were measured in Gjb2 cKO mice (n=4 animals) and littermate controls (n=6 animals) at 5 different auditory frequencies (mean ± SEM).

582 Unlike littermate controls, Gjb2 cKO animals had no response at any frequency, even at the
583 highest sound level tested (80 dB).
584 **B)** ABR thresholds to a broadband frequency "click" were measured in Gjb2 cKO mice (n=4
585 animals) and littermate controls (n=6 animals). Gjb2 cKO animals had no response, even at the
586 highest sound level tested (80 dB).
587 **C)** Distortion product otoacoustic emissions (DPOAE) thresholds, which are sounds generated
588 by mechanically active cells in the ear in response to sound stimuli, were measured in Gjb2 cKO
589 mice (n=4 animals) and littermate controls (n=6 animals) for 8 different frequency pairs (mean ±
590 SEM). Gjb2 cKO animals had no DPOAE at any frequency, even at the highest sound level
591 tested (75 dB).
592 **D)** Example neurons responding to white noise at varying sound levels (dB) in anesthetized
593 littermate control and Gjb2 cKO mice. Each row corresponds to an individual neuron.
594 **E)** Average change in firing rate of neurons (mean ± SE) in littermate control (n=13 neurons
595 from 2 mice) and Gjb2 cKO mice (n=9 neurons from 2 mice) to white noise at varying sound
596 intensities.
597 **F)** Force-frequency heat maps in response to vibration of differing frequencies and intensities in
598 two neurons from littermate controls and two neurons from Gjb2 cKO mice.
599 **G)** Average force-frequency threshold curves of LCIC neurons (mean ± 95% confidence
600 interval) recorded in control (n=9 neurons from 2 animals), and Gjb2 cKO mice (n=11 neurons
601 from 2 animals). Thresholds between Gjb2 cKO and controls were not significantly different
602 (Mann-Whitney U Test with Bonferroni correction for multiple comparisons).

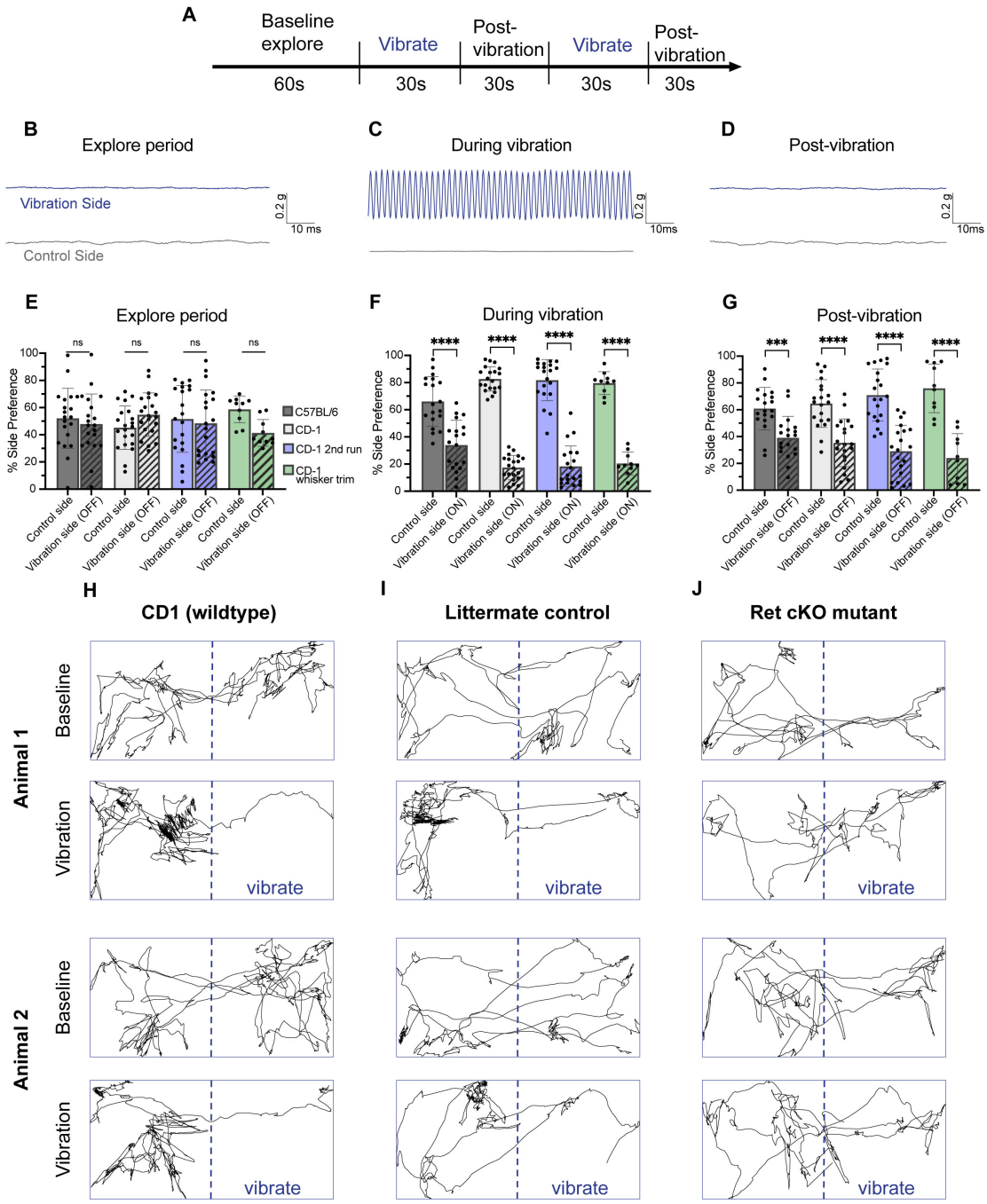

Extended Data Figure 9: A place preference behavioral assay for measuring behavioral responses to 500 Hz vibration of a platform.

A) Timeline of behavioral trial.

B-D) Accelerometer traces from vibration side (blue) and control side (gray) of the behavioral chamber during the baseline period (B), vibration period (C), and post-vibration period (D) of the

609 behavioral trial. Amplitude of the platform vibration was ~ 0.3 g (gravitational force) when the
610 vibration stimulus was on.
611 **E-G**) Percent of time spent that mice spent on the control and vibration side of the chamber
612 during the explore period (E), vibration period (F), and post-vibration period (G) of the
613 behavioral trial for four different conditions: naïve C57BL/6 mice (n=19 animals), naïve CD-1
614 mice (n=20 animals), CD-1 mice run on the behavior for the second time, one week later (n=20
615 animals), and naïve CD-1 mice that had been whisker trimmed (n=10 animals; ***$p<0.001$,
616 ****$p<0.0001$, paired t-test).
617 **H-J)** Representative activity traces of two example wildtype CD-1 animals (H), littermate
618 control animals (I), and Ret cKO animals (J), tracking movement during the baseline and
619 vibration periods.

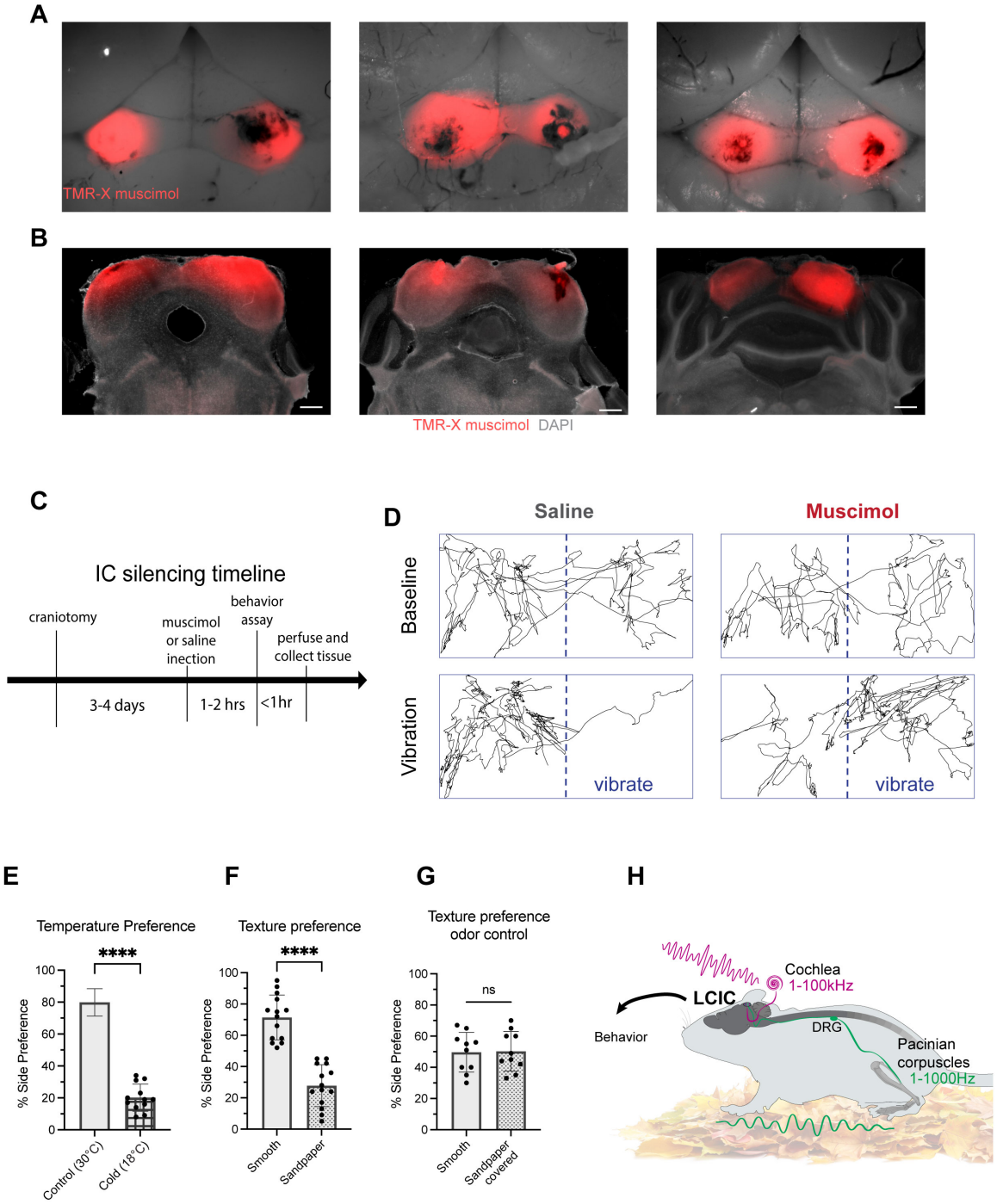

Extended Data Figure 10: Behavioral and anatomical characterization of LCIC silenced mice.

A) Post-hoc histology of three different TMR-X conjugated muscimol injected animals, showing restriction of the injection to the inferior colliculus.

B) Coronal sections of a representative TMR-X conjugated muscimol injected brain to show ventral spread of the injection. Scale bar = 500 μm.

C) Timeline of IC silencing experiments.

D) An additional example activity trace from a saline injected control and muscimol injected animal, showing movement during the baseline and vibration period of the behavioral trial.

E) Temperature preference assay done for naïve wildtype CD-1 animals (n=10 animals, ****$p<0.0001$, unpaired t-test). Note, this is a separate cohort from the group used in silencing experiments, reported in Fig. 4.

F) Texture preference assay done for naïve CD-1 animals (n=10 animals, ****$p<0.0001$, unpaired t-test). Note, this is a separate cohort from the group used in silencing experiments in Fig. 4.

E) Some types of sandpaper are aversive to mice due to their odor. To ensure our texture avoidance behavioral measure reflects avoidance of an aversive texture and not odor, the sandpaper was covered by a smooth paper with small holes punched in it, such that the odor of the paper could be sensed, but the texture could not be felt. In this condition, mice (n=10 animals) did not demonstrate an aversion to the sandpaper side. (Not significant, paired t-test.)

H) A model in which the LCIC integrates auditory cues detected by the cochlea and vibrotactile cues detected by Pacinian corpuscles to drive behavioral responses to vibration.

643 **Methods**

644

645 **Animals**

646 *Avil*^{Cre}, *TrkB*^{flox}, *Ret*$^{flox(eGFP)}$, and *Vglut2*^{Cre} mouse lines were of mixed background (CD-1 and
647 C57BL/6J). *Gjb2*^{flox} and *Sox10*^{Cre} were on a C57BL/6 background. CD-1 animals were imported
648 from Charles River (#022) and C57BL/6 animals were imported from The Jackson Laboratory
649 (#000664). The following mouse lines have been previously described, including: *Sox10*^{Cre} (Ref:
650 77, Jax 025807), *Avil*^{Cre}(Ref: 78, JAX 032536), *TrkB*^{flox}(Ref:79), *Ret*$^{flox(eGFP)}$ (JAX 029846), and
651 *Vglut2*^{Cre} (JAX 016963). The *Gjb2*^{flox} mouse line, in which loxP sites flank the entire coding
652 sequence in exon 2, was generated by KTB in the laboratory of DPC and will be described
653 elsewhere. Mice were handled and housed in standard cages in accordance with Harvard Medical
654 School and IACUC guidelines. Both male and female mice were used in all experiments. Control
655 littermates of *Ret*, *TrkB,* and *Gjb2* conditional mutants included Cre-negative animals that were
656 negative, heterozygous, or homozygous for the floxed allele. Our data indicated no difference
657 among controls of different genotypes; therefore, they were combined for statistical analyses and
658 collectively referred to as "controls."

659

660 **Perfusions**

661 Mice were anesthetized under isoflurane and transcardially perfused with 5-10 mL of PBS,
662 followed by 5-10 mL of 4% paraformaldehyde (PFA) in PBS. After perfusion, the skull was
663 removed and post-fixed in 4% PFA in PBS at 4°C overnight. Skin samples were removed and
664 fixed overnight in Zamboni's fixation buffer with gentle agitation at 4°C. Samples were washed
665 3x10 min in PBS at room temperature after overnight fixation before fine dissection.

666

667 **Immunohistochemistry of skin cryosections, brain cryosections and whole-mount tissue**

668 The following dilutions and primary antibodies were used: chicken anti-NFH (Aves # NFH,
669 1:500), rabbit anti-S100 Beta (VWR/Protein Tech #15146-1-AP, 1:300), rabbit anti-dsRed
670 (Takara #632496. 1:1000), chicken anti-GFP (Abcam #13970, 1:1000), goat anti-GFP (US
671 Biological Life Sciences # G8965-01E, 1:500). The secondary antibodies used were Alexa 488,
672 546 or 647 conjugated donkey or goat anti-rabbit, chicken, or goat (Life Technologies or Jackson
673 ImmunoResearch) and were prepared at 1:500 or 1:1000 dilutions.

For Meissner corpuscle histology, paws were removed from perfused mice. The pads and fingertips were clipped off of the glabrous skin using small spring scissors and cryoprotected in 30% sucrose in PBS at 4 °C for 1-2 days, embedded in OCT (1437365, Fisher), frozen using dry ice, and stored at −80 °C. The tissues were cryosectioned (25 μm) using a cryostat (Leica) and collected on glass slides (12-550-15, Fisher). Sections were washed 3 times for 5 minutes each with PBS containing 0.1% Triton X-100 (0.1% PBST), incubated with blocking solutions (0.1% PBST containing 5% normal goat serum (S-1000, Vector Labs) or normal donkey serum (005-000-121, Jackson Immuno) for 1 hour at room temperature, incubated with primary antibodies diluted in blocking solutions at 4 °C overnight, washed 3 times for 10 minutes each with 0.1% PBST, incubated with secondary antibodies diluted in blocking solutions at 4 °C overnight, washed again 4 times for 10 minutes each with 0.1% PBST (DAPI solution was included in the second wash at 1:5000 dilution), and mounted in Fluoromount-G mounting medium (Fisher 0100-01).

For whole-mount staining of Pacinian corpuscles, animals were anesthetized under isoflurane and euthanized by cervical dislocation. For Pacinian corpuscle dissections, the tibia and fibula of the ankle, and radius and ulna of the wrists were dissected immediately after euthanasia, keeping muscle and surrounding tissue intact, and fixed overnight in Zamboni's fixative at 4 °C. Limbs were washed 3x10 minutes in PBS and then finely dissected to remove muscle on the bone, while leaving the interosseous membrane of the bone intact. Tissues were then washed every 30 minutes for 5-6 hours with 1% PBST (PBS + triton X-100). Primary antibodies were applied in blocking solution (5% normal goat or donkey serum, 75% PBST, 20% DMSO, 0.01% NaN3) and incubated at room temperature for 3-5 nights with gentle rocking. Tissues were rinsed 3x in PBST, then washed every 30 minutes for 5-6 hours in 1% PBST. Secondary antibodies were applied in blocking solution and incubated at room temperature for 3-5 nights, with gentle rocking. Tissues were rinsed 3x in 1% PBST, washed every 30 minutes for 5-6 hours in 1% PBST, then serially dehydrated (10-15 minutes per wash) in 50%, 75%, and 100% ethanol diluted in distilled water. Tissue was stored at -20 °C in 100% ethanol until clearing and imaging. Tissue was cleared in BABB (1 part benzyl alcohol to 2 parts benzyl benzoate) for 2-12 hours at room temperature and mounted in BABB for imaging. For mounting, chambers were

705 made on slides consisting of a thin layer of vacuum grease to create four walls followed by
706 placement of a coverslip. Tissue was imaged on a Zeiss LSM 900 confocal microscope using the
707 10x objective.
708
709 For brain sections, brains were cryoprotected in 30% sucrose overnight. Tissue was
710 cryosectioned (50 uM sections) and collected in a 12-well plate filled with PBS. Sections were
711 stained free floating using a 12-well plate. Sections were washed 3x5 minutes each with 1x PBS
712 containing 0.1% Triton X-100 (0.1% PBST), incubated with blocking solutions (0.1% PBST
713 containing 5% normal goat serum (S-1000, Vector Labs) or normal donkey serum (005-000-121,
714 Jackson Immuno) for 1-2 hours at room temperature, incubated with primary antibodies diluted
715 in blocking solutions at 4 °C overnight. Subsequently, sections were washed 3x10 minutes each
716 with 0.1% PBST, incubated with secondary antibodies diluted in blocking solutions at room
717 temperature for 2 hours, and washed again 4x10 minutes each with 0.1% PBST (DAPI solution
718 was included in the second wash at 1:5000 dilution). Sections were mounted onto glass slides
719 and coverslipped in Vectashield (Vector Labs).
720
721 **Quantification of peripheral anatomy**
722 For quantification of Meissner corpuscles in Ret cKO mice and littermate controls, cryosectioned
723 and stained skin from the pads and fingertips were imaged with a widefield Zeiss LSM 700
724 microscope. Images of sections were analyzed in the Fiji distribution of Image J (www.fiji.sc). In
725 each section, the number of Meissner corpuscles, visualized by S100 antibody staining, were
726 counted. The length of the surface of the skin was traced and measured in ImageJ, and density
727 was calculated by dividing the number of Meissner corpuscles by the length of the skin surface.
728 Quantification was done blind to genotype.
729
730 For quantification of Pacinian corpuscles in Ret cKO mice, TrkB cKO mice, and littermate
731 controls, images of stained and intact limbs were taken using a Zeiss LSM 900 confocal
732 microscope using the 10x objective. The number of Pacinian corpuscles, visualized by S100
733 antibody staining, were counted. Quantification was done blind to genotype.
734
735 **DRG recordings**

736 Animals were anesthetized with urethane (1.5 g/kg) or isoflurane (1.5-2%). A skin incision was
737 made over the L3-L5 vertebrae and muscle surrounding the vertebrae was removed. The L3 and
738 L5 vertebrae were fixed in place using custom-built clamps. The L4 DRG was exposed by
739 removing overlaying bone. A borosilicate glass electrode (1 MΩ) was lowered into the DRG
740 using a motorized manipulator (Scientifica) to search for units. Recordings were amplified using
741 a MultiClamp 700B (Molecular Devices) under the 100x AC differential amplification mode
742 with additional 20x gain. Signals were collected with a 0.1 kHz high-pass filter and 3 kHz Bessel
743 filter, and acquired using a Digidata 1550B (Molecular Devices) sampled at 20 kHz. For
744 Pacinian corpuscle innervating Aβ-RA2-LTMRs, a search stimulus of 300 Hz vibration (40 mN)
745 was applied to the ankle. Pacinians were identified by their large receptive fields, and their end
746 organ location on the fibula was identified through electrical stimulation following
747 measurements of their vibration tuning. For Meissner corpuscle innervating Aβ-RA1-LTMRs,
748 the hindlimb digits were brushed as the electrode was descended. Aβ-RA1-LTMRs were
749 identified by their small skin receptive fields, adapting responses to indentation, low mechanical
750 thresholds (<10 mN), and cutaneous endings that could be excited by electrical stimulation of the
751 skin. Vibrations (10-900 Hz) of varying intensity (1-50 mN) were delivered to the most sensitive
752 area of the receptive field for each unit, collecting at least 4 trials per force for each frequency.
753

754 **Craniotomies for MEA recordings**

755 Mice were injected with sustained release buprenorphine (0.1 mg/kg), anesthetized with
756 isoflurane, and placed in a small animal stereotaxic frame (David Kopf Instruments). A titanium
757 headplate was cemented to the mouse's skull (C&B Metabond). A craniotomy was made
758 centered over the right inferior colliculus (stereotaxic coordinates: 0.5 mm posterior, 1.8 mm
759 lateral of lambda), or centered over the right VPL (stereotaxic coordinates: 1.7 mm posterior,
760 1.9 mm lateral of bregma), keeping the dura intact. Kwik-sil adhesive (World Precision
761 Instruments) was used to cover the craniotomy until the day of recording (within 3 days of the
762 craniotomy).
763

764 **Multielectrode array (MEA) recordings**

765 For anesthetized recordings, the mouse was injected intraperitoneally with urethane (0.5-
766 1.5 mg/g), placed on a heated platform, and head fixed such that the paws on the side

contralateral to the craniotomy were accessible for mechanical stimulation. MEAs were inserted into the LCIC (H6b-32ch or H7b-32ch, Cambridge Neurotech) or VPL (H6b-32ch, H7b-32ch, or E4-64ch, Cambridge Neurotech) with a 3-axes micromanipulator (IVM mini, Scientifica). MEA signals were high-pass filtered at 200 Hz, amplified (RHD2132), and acquired at 20 kHz (RHD2000, Intantech) for offline processing.

For VPL recordings, hindlimb VPL was targeted using coordinates (1.6 mm posterior, 1.9 mm lateral to bregma), and the location was verified by brushing the hindlimb. The LCIC was targeted by positioning the MEA probe posterior to the transverse sinus and ~1.6-1.8 mm lateral, with a 45-degree angle to insert the probe underneath the transverse sinus. In preliminary experiments, probe penetrations that contained only auditory responsive neurons were shown to be in the CNIC, unlike penetrations in the LCIC that contained both mechanical and auditory responses. Therefore, subsequent penetrations that contained only auditory responses were assumed to be in the CNIC and were not included in the analysis. For verification of recording location, after recording was complete, the probe was lifted from the brain, the probe was coated with DiI (Thermo Fisher) then re-inserted to the same coordinates, and the brain was collected and post-fixed overnight in 4% PFA post-recording. Recordings were performed and analyzed blind to genotype.

Force-frequency tuning experiments (anesthetized): The receptive fields for neurons on the probe were determined by gently brushing the digits or pads using a fine paintbrush. The paw was fixed to the platform with Easy Mold Silicone Putty (Environmental Technologies). The mechanical stimulator (with a blunt 1 mm probe) was then targeted to the receptive fields identified by brush. In the case of LCIC neurons, which had large receptive fields that lacked a hotspot, the probe was targeted to the heel of the hindlimb. As above, for verification of recording location, after recording was complete, the probe was lifted from the brain, the probe was coated with DiI (Thermo Fisher) then re-inserted to the same coordinates, and the brain was collected and post-fixed overnight in 4% PFA post-recording. Thresholds for each vibratory frequency were defined as the force required to elicit 20% of a unit's maximum firing during the sustained portion of the stimulus (200 ms window beginning 50 ms after stimulus onset).

797 *VPL and LCIC mapping experiments (anesthetized):* For VPL mapping experiments (Extended
798 Data Fig. 3) a 4 shanked probe (E4-64 ch, Cambridge Neurotech) was positioned with the shanks
799 aligned to the anterio-posterior axis. Mapping began medially (at ~1.7 mm lateral) and moved
800 100 μm lateral for each successive penetration. For each probe penetration, the contralateral
801 hindlimb, thigh, trunk, forelimb, and face were stroked with a paintbrush. The hindlimb was
802 fixed to the platform with Easy Mold Silicone Putty and stimulation at 50 Hz and 500 Hz was
803 delivered to the hindpaw with a 10 mN intensity using a mechanical stimulator with a wide blunt
804 tip (3 mm diameter). Complementary LCIC experiments used a single shank probe (H6b or H7b,
805 Cambridge Neurotech), with probe penetrations also separated by 100 μm intervals. Before each
806 probe penetration the probe was coated with DiI and recording locations were verified post-
807 experiment. Neurons were considered brush responsive to a body region if their change in firing
808 exceeded 10 Hz during the brush period. Similarly, neurons were considered responsive to 500
809 Hz vibration if their change in firing exceeded 10 Hz during the sustained portion (200 ms time
810 period beginning 50 ms after stimulus onset) of the stimulus.

811 *Awake LCIC recordings:* For awake LCIC recordings, animals were head-fixed, and the LCIC
812 was targeted as described above. Mechanical stimulation was targeted to the platform the animal
813 stood on rather than the limb. The platform was made of thin (1/8") acrylic. Trials where the
814 animal was moving were excluded.

815 **Mechanical and auditory stimuli**

816 For *in vivo* electrophysiology, vibrations were generated using a DC motor with a blunt 1-mm or
817 3-mm diameter probe, as previously described[5,28]. The motor was driven by a custom-built
818 current supply controlled by Wavesurfer and a multifunction I/O board (USB-6343, National
819 Instruments), and static forces calibrated using a fine scale. For awake recordings, the
820 mechanical stimulator was covered with a sound dampening foam tip, and placed underneath the
821 acrylic platform the animal stands on. The magnitude of vibration was measured using an
822 accelerometer attached to the bottom of the platform and reported in units of gravitational force
823 (g). Brush stimuli were manually delivered with a 4 mm diameter brush at a rate of one stroke
824 per 2 seconds in the rostral to caudal direction.
825

826 Auditory stimuli were amplified by an SA1 stereo power amplifier (Tucker-Davis Technologies)
827 and delivered through an MF1 multi-field magnetic speaker (Tucker-Davis Technologies),
828 positioned 14 cm from the ear contralateral to recording site. Auditory stimuli were generated in
829 MATLAB and delivered using WaveSurfer and a multifunction I/O board (USB-6343, National
830 Instruments). Broadband (white) noise (0-50 kHz) was delivered in 100 ms pulses (5 ms rise-fall
831 time) at 65 dB SPL. White noise, vibration, and combined trials were interleaved. For awake
832 recordings, trials where the animal was moving were excluded.
833
834 **Spike detection and cluster assignment**
835 Data was converted into contiguous binary files (https://github.com/peltonen/kwik-tools) and
836 processed using JRClust (Janelia). Spikes were detected and assigned to clusters corresponding
837 to individual or multiples units with JRClust (https://github.com/JaneliaSciComp/JRCLUST).
838 These initial clusters were manually curated to remove artifacts that did not correspond to spike
839 waveforms, and clusters were examined and split if their PCA decompositions were not
840 monodispersed. This collection of clusters was then examined and merge operations performed if
841 consideration of the average spike waveform and spiking cross-correlation indicated that two
842 clusters corresponded to the same neuron. Manual curation typically resulted in putative isolated
843 single units with intra-cluster waveform correlations greater than 0.9, inter-cluster waveform
844 correlations less than 0.1, and clusters that did not meet these criteria were not considered in the
845 dataset. Spike event times for each cluster were exported and processed in Python.
846
847 **Anterograde tracing experiments**
848 For anterograde tracing experiments (Extended Data Fig. 1), brainstem DCN neurons of
849 *Slc17a6*^{Cre} (Vglut2) mice were transduced with either an AAV encoding synaptophysin-GFP,
850 AAV1-CAG-FLEX-Synaptophysin-GFP-WPRE (1.088E+14gc/ml), or synaptophysin-tDT,
851 AAV1-CAG-FLEX-Synaptophysin-tdTomato-WPRE (1.1482E+14gc/ml). Viruses were
852 produced and packaged at the Boston Children's Hospital Viral Core Facility. Mice were
853 injected with sustained release buprenorphine (0.1 mg/kg), anesthetized with isoflurane and
854 placed in a small animal stereotaxic frame (David Kopf Instruments) with their neck bent at a 45
855 degree angle. The dorsal column nuclei were exposed between the base of the skull and C1
856 through retraction of the paraspinal muscles. A small nick in the overlying dural membrane was

857 made to allow access for the injection pipette. A borosilicate glass pipette was lowered to a depth
858 of 0.5 mm in either the gracile (0.1 mm lateral to obex) or cuneate (0.5mm anterior to obex, 0.1
859 mm lateral to fourth ventricle) nucleus. 50-100 nL of AAV virus with fast green was injected at a
860 rate of 50 nL min−1 using a Microinject system (World Precision Instruments). Three weeks
861 after injection, mice were perfused, and brain tissue was collected for cryosectioning and
862 immunohistochemistry.
863
864 **Auditory brainstem responses (ABR) and distortion product otoacoustic emissions**
865 **(DPOAE)**
866 All measurements and analyses were conducted blind to the animal's experimental condition.
867 For anesthesia, mice were given an IP injection of ketamine (100 mg/kg body weight, BW),
868 xylazine (10 mg/kg BW) and acepromazine (0.3 mg/kg BW) and placed on their side on a 37°C
869 metal heating pad (ATC-2000, World Precision Instruments). Experiments were performed in a
870 sound-attenuating, electrically shielded chamber (IAC Acoustics). After anesthesia induction,
871 eye lubricant (GenTeal Tears, Alcon) was applied to prevent drying. A ketamine boost (0.3 – 0.5
872 mg/kg BW) was used to maintain anesthesia at the first sign of movement or elevation in the
873 signal rejection rate (rejection threshold was 15 μV).
874
875 An acoustic system consisting of a microphone and dual earphone assembly coupled to a probe
876 tube was used to deliver and measure acoustic stimuli. This custom system was built by the
877 Engineering Core of the Eaton-Peabody Laboratories (EPL) at Massachusetts Eye and Ear
878 (MEE) (Boston). The probe end of the acoustic system was placed ~1 mm over the center of the
879 ear canal. Stimuli were digitally generated and then amplified by an SA1 stereo power amp
880 (Tucker Davis Technologies) to drive the acoustic system. The probe tube microphone was
881 amplified by a custom microphone amplifier (EPL at MEE) and sent to a 24-bit I/O board (PXI-
882 4461) installed into a PXI chassis (PXIe-1073, National Instruments).
883
884 Bioelectrical signals were recorded using three subdermal electrodes: an active electrode at the
885 vertex, a reference electrode near the pinna, and a ground electrode near the tail. Signals were
886 passed through a custom pre-amplifier (EPL at MEE) before digitization. Acoustic stimuli
887 consisted of clicks and 5 ms tone pips with a repetition rate of 30 s^{-1} and a 0.5 ms rise-fall time at

888 the following frequencies (in kHz): 8, 16, 22.6, and 32. Stimuli were presented in alternating
889 polarity to cancel out the cochlear microphonic potential. Cochlear Function Test Suite (CFTS)
890 software (version 2.37.2; MEE, Boston) amplified (x104), filtered (0.3–3 kHz passband), and
891 averaged 512 responses at each sound pressure level (SPL). ABR thresholds were manually
892 designated blind to genotype using the ABR Peak Analysis Software from the EPL at MEE.
893
894 DPOAEs were recorded in response to primary tones f1 and f2 at a frequency ratio of f2/f1 = 1.2,
895 and a SPL level of L1 = L2 + 10 dB. For individual DPOAE trials, f2 consisted of 5.6, 8, 11.3,
896 16, 22.6, 32, 42.5, or 64 kHz tones that were incremented in 10 dB steps from 10 to 70 dB SPL.
897 The cubic distortion product 2f1-f2 was extracted by Fourier analysis of the ear-canal sound
898 pressure after waveform and spectral averaging. DPOAE threshold was defined as the f1 level
899 required to produce a DPOAE of 5 dB SPL, except at 64 kHz where the threshold was defined as
900 10 dB SPL due to a higher noise floor.
901
902 **Muscimol silencing**
903 For muscimol silencing experiments, mice were injected with sustained release buprenorphine
904 (0.1 mg/kg), anesthetized with isoflurane, and placed in a small animal stereotaxic frame (David
905 Kopf Instruments). A small section of skin above the rear of the skull was removed with surgical
906 scissors and the skull was dried. The skin was glued to the skull using Vetbond (3M healthcare),
907 and a small amount of dental cement (C&B Metabond) was used to cover the exposed region of
908 the skull, leaving the area where the craniotomy would be drilled clear. A small craniotomy was
909 drilled approximately 0.5 mm posterior, 1.8 mm lateral to lambda. The craniotomy was covered
910 with Kwik-sil adhesive.
911
912 Animals were given 3-4 days to recover. On the day of the behavioral experiment, animals were
913 anesthetized with isoflurane and placed in a small animal stereotaxic frame. A borosilicate glass
914 pipette was used to bilaterally inject into the inferior colliculus (0.5-0.8 mm posterior to lambda,
915 1.5-1.8 mm lateral, 0.5 mm deep) with TMR-X muscimol dissolved in ACSF (1.5 mM,
916 Invitrogen M23400). 50 nL injections were made in two locations per side (100 nL total per
917 side). Control mice received the same injection volume of sterile saline. Injections were
918 performed at a rate of 50 nL min−1 using a Microinject system (World Precision Instruments)

and the pipette was allowed to sit in the brain for 3 minutes post-injection. Animals were allowed to recover from isoflurane and habituate to the behavior room for ~1 hour, and the behavioral assay (vibration, temperature, or texture) was run within 2 hours. Behavioral assays were run blind to experimental group (saline or muscimol). Post-behavior, animals were perfused. Muscimol spread was confirmed post-hoc following vibratome sectioning the brain and imaging.

Behavior methods for Openfield, Vibration Platform and Temperature Preference assays

To reduce anxiety and improve handling, animals were enriched with Bio-Serv igloos, tunnels or chew shacks at least one month prior to all behavior testing. One week prior to behavioral testing, animals were moved to the testing room and home cage habituated to the behavior room to acclimate to room lighting (warm white, 2700k), sound (ambient 45-50 dB), odor (cleaned with ECOS unscented dish soap and 70% EtOH), and temperature (73 ^{o}F, 30% humidity). Vibration, temperature, and texture assays were conducted in 3-4 month old CD-1 animals (unless otherwise noted). Vibration assays in Ret cKO and littermate controls were performed at 8 weeks of age and were performed blind to genotype.

Vibration Platform and Sound Only Test: Two days prior to testing, animals were moved to the testing room and habituated to investigator handling. Animals were group habituated to the black matte test chamber (12 in L x 6 in W x 7 in H x 0.25 in), center divided with an arched doorway and allowed to freely explore for 5 minutes. During the three-day room/chamber habituation, animals were also habituated to the vibration motor sound only. The vibration platform was elevated 6 inches above the base. Two flat surface vibration motors, (PUI Audo, ASX08604-SW-R 4 ohm, BST) were suspended above the base, resting on spring mounted posts, one motor on each side of the chamber to act as the suspension base for the two square white matte acrylic floors, (5.5 in L x 5.5 in W x 0.125 in D) to rest on and provide vibration stimulus to each floor when activated. The acrylic floors were separated by a thin gap and lightly attached to the motor. An accelerometer was attached to each floor to ensure vibration floor displacement was constant for each test animal. The entire floor was covered with a thin stretch white matte cloth napkin (WypAll L30, 05812) to prevent the animals from investigating the gap in the floor and edges of the chamber walls as well as maintain a clean odor free test environment. The black matte acrylic test chamber rested on four pillars (6 inches above the floor) to ensure the chamber walls snugly surrounded the vibration floors without direct contact to prevent the

chamber from vibrating when the motor was activated during testing. The room and test platform were lined with odorless 1-inch thick Bonded Logic Natural Fiber Acoustic Sound Absorbing panels (Model #60600-11212).

Vibration Test: The test chamber was modified on test day by removing the front and side wall to create a semi-open and closed end (L-shape) to increase animals' awareness of the floor surface when exploring both sides of the test chamber. The center divider with open doorway was left in place. The semi-closed side of the chamber was the non-stimulus side and the semi-open side was the vibration stimulus side. A custom Bonsai script was used to trigger the vibration motor and camera. The three-minute vibration test sequence was as follows: The animal was placed in the chamber facing the semi-open side which encouraged the animal to walk through the doorway and explore the newly semi-closed side of the chamber.
Stage-1: Start, allow one minute baseline explore of test chamber,
Stage-2: 30 second vibration stimulus on the semi-open side,
Stage-3: 30 second interim period with no stimulus,
Stage-4: 30 second vibration stimulus on the semi-open side,
Stage-5: 30 second final period with no stimulus.

For the sound only test, the motor was disconnected from floor contact and the motor sound only was played for the 30 second stimulus during stage-2 and stage-4. Ambient room and chamber decibel level was 45-50 dB. During sound only and vibration stimulus periods, the background sound in the testing room and chamber was set to 70 dB at 500 Hz. A top video recording device was used to track distance traveled and time exploring the two chambers.

Temperature Preference Test: Two days prior to testing, animals were moved to the testing room and home cage habituated to the behavior. Animals were group habituated for 5 minutes to the black matte test chamber (12 in L x 6 in W x 7 in H x 0.25 in), center divided with an arched doorway, resting on two metal plate floors (5.5 in L x 5.5 in W ea) both set to neutral temperature 30 ^{o}C. On the third day following room habituation, each animal was tested on contrasting temperatures, 30 ^{o}C (warm) vs 18 ^{o}C (cold). Each animal was placed in the test chamber on the warm side facing the doorway to the cold side to encourage the animals to walk

through the doorway and freely explore both temperatures for 5 minutes. A top video recording device was used to track distance traveled and time exploring the two chambers.

Texture Preference Assay: Two days prior to testing, animals were moved to the testing room and home cage habituated to the behavior. Animals were group habituated for 10 minutes to the black matte test chamber (12 in L x 6 in W x 7 in H x 0.25 in) with no divider. On the third day following room habituation, each animal was tested on contrasting floors, construction paper (Tru-Ray Heavyweight, Pacon) vs coarse 60-grit sandpaper (ceramic version, 26060PGP-4, 3M). There was no divider between the smooth and rough textured floors. Each animal was placed in the test chamber on the smooth side and animals were given 10 minutes to freely explore both chambers. A top video recording was used to track distance traveled and time exploring the two chambers.

Quantification and statistical analysis

Statistical tests were conducted in Python 3.7.9 using the SciPy stats module or in GraphPad Prism. Normality of the data was tested using the Shapiro-Wilk test. Comparisons between two independent groups were performed using the unpaired t-test (in the case of two groups distributed normally, with no significant difference between variances), Welch's t-test (in the case of two groups distributed normally, but with unequal variances), or Mann-Whitney test (non-parametric data). When correction for multiple comparisons was necessary, the Bonferroni correction was used. An adjusted p value < 0.05 was considered significant. Additional details on sample sizes and statistical tests for each experiment can be found in figure legends and the main text.

1004 **References**

1005 1. Pickles JO. Auditory pathways: anatomy and physiology. *Handb Clin Neurol.*
1006 2015;129:3-25.
1007 2. Handler A, Ginty DD. The mechanosensory neurons of touch and their mechanisms of
1008 activation. *Nat Rev Neurosci.* 2021;22(9):521-537.
1009 3. Sato M. Response of Pacinian corpuscles to sinusoidal vibration. *J Physiol.*
1010 1961;159(3):391-409.
1011 4. Bolanowski SJ, Jr., Zwislocki JJ. Intensity and frequency characteristics of pacinian
1012 corpuscles. II. Receptor potentials. *J Neurophysiol.* 1984;51(4):812-830.
1013 5. Turecek J, Ginty DD. Coding of self and environment by Pacinian neurons in freely
1014 moving animals. *bioRxiv.* 2023.
1015 6. Cividini S, Sfenthourakis S, Montesanto G. Are terrestrial isopods able to use stridulation
1016 and vibrational communication as forms of intra and interspecific signaling and defense
1017 strategies as insects do? A preliminary study in Armadillo officinalis.
1018 *Naturwissenschaften.* 2019;107(1):4.
1019 7. Narins PM, Reichman OJ, Jarvis JU, Lewis ER. Seismic signal transmission between
1020 burrows of the Cape mole-rat, Georychus capensis. *J Comp Physiol A.* 1992;170(1):13-
1021 21.
1022 8. Nevo E, Heth G, Pratt H. Seismic communication in a blind subterranean mammal: a
1023 major somatosensory mechanism in adaptive evolution underground. *Proc Natl Acad Sci*
1024 *U S A.* 1991;88(4):1256-1260.
1025 9. O'Connell-Rodwell CE. Keeping an "ear" to the ground: seismic communication in
1026 elephants. *Physiology (Bethesda).* 2007;22:287-294.
1027 10. Virant-Doberlet M, Stritih-Peljhan N, Zunic-Kosi A, Polajnar J. Functional Diversity of
1028 Vibrational Signaling Systems in Insects. *Annu Rev Entomol.* 2023;68:191-210.
1029 11. Johnson KO. The roles and functions of cutaneous mechanoreceptors. *Curr Opin*
1030 *Neurobiol.* 2001;11(4):455-461.
1031 12. Heffner RS, Koay G, Heffner HE. Audiograms of five species of rodents: implications for
1032 the evolution of hearing and the perception of pitch. *Hear Res.* 2001;157(1-2):138-152.
1033 13. Heffner HE, Heffner RS. Hearing ranges of laboratory animals. *J Am Assoc Lab Anim*
1034 *Sci.* 2007;46(1):20-22.

1035 14. Yau JM, Olenczak JB, Dammann JF, Bensmaia SJ. Temporal frequency channels are
1036 linked across audition and touch. *Curr Biol.* 2009;19(7):561-566.
1037 15. Neubarth NL, Emanuel AJ, Liu Y, et al. Meissner corpuscles and their spatially
1038 intermingled afferents underlie gentle touch perception. *Science.* 2020;368(6497).
1039 16. Prsa M, Morandell K, Cuenu G, Huber D. Feature-selective encoding of substrate
1040 vibrations in the forelimb somatosensory cortex. *Nature.* 2019;567(7748):384-388.
1041 17. Lee K-S, Wagner DdT, Sanders M, Huber D. Emergence of a somatosensory tonotopic
1042 map for substrate vibration in the brainstem. *bioRxiv.* 2023.
1043 18. Bouley DM, Alarcon CN, Hildebrandt T, O'Connell-Rodwell CE. The distribution,
1044 density and three-dimensional histomorphology of Pacinian corpuscles in the foot of the
1045 Asian elephant (Elephas maximus) and their potential role in seismic communication. *J*
1046 *Anat.* 2007;211(4):428-435.
1047 19. Germann C, Sutter R, Nanz D. Novel observations of Pacinian corpuscle distribution in
1048 the hands and feet based on high-resolution 7-T MRI in healthy volunteers. *Skeletal*
1049 *Radiol.* 2021;50(6):1249-1255.
1050 20. Kumamoto K, Senuma H, Ebara S, Matsuura T. Distribution of pacinian corpuscles in the
1051 hand of the monkey, Macaca fuscata. *J Anat.* 1993;183 (Pt 1)(Pt 1):149-154.
1052 21. Silfvenius H. Characteristics of receptors and afferent fibers of the forelimb interosseous
1053 nerve of the cat. *Acta Physiol Scand.* 1970;79(1):6-23.
1054 22. Zelena J. The development of Pacinian corpuscles. *J Neurocytol.* 1978;7(1):71-91.
1055 23. Hulliger M, Nordh E, Thelin AE, Vallbo AB. The responses of afferent fibres from the
1056 glabrous skin of the hand during voluntary finger movements in man. *J Physiol.*
1057 1979;291:233-249.
1058 24. Salinas E, Hernandez A, Zainos A, Romo R. Periodicity and firing rate as candidate
1059 neural codes for the frequency of vibrotactile stimuli. *J Neurosci.* 2000;20(14):5503-
1060 5515.
1061 25. Luna R, Hernandez A, Brody CD, Romo R. Neural codes for perceptual discrimination in
1062 primary somatosensory cortex. *Nat Neurosci.* 2005;8(9):1210-1219.
1063 26. Harvey MA, Saal HP, Dammann JF, 3rd, Bensmaia SJ. Multiplexing stimulus
1064 information through rate and temporal codes in primate somatosensory cortex. *PLoS Biol.*
1065 2013;11(5):e1001558.

1066 27. Abraira VE, Ginty DD. The sensory neurons of touch. *Neuron.* 2013;79(4):618-639.
1067 28. Turecek J, Lehnert BP, Ginty DD. The encoding of touch by somatotopically aligned
1068 dorsal column subdivisions. *Nature.* 2022;612(7939):310-315.
1069 29. Aitkin LM, Dickhaus H, Schult W, Zimmermann M. External nucleus of inferior
1070 colliculus: auditory and spinal somatosensory afferents and their interactions. *J*
1071 *Neurophysiol.* 1978;41(4):837-847.
1072 30. Aitkin LM, Kenyon CE, Philpott P. The representation of the auditory and somatosensory
1073 systems in the external nucleus of the cat inferior colliculus. *J Comp Neurol.*
1074 1981;196(1):25-40.
1075 31. Aitkin LM, Webster WR, Veale JL, Crosby DC. Inferior colliculus. I. Comparison of
1076 response properties of neurons in central, pericentral, and external nuclei of adult cat. *J*
1077 *Neurophysiol.* 1975;38(5):1196-1207.
1078 32. Bjorkeland M, Boivie J. An anatomical study of the projections from the dorsal column
1079 nuclei to the midbrain in cat. *Anat Embryol (Berl).* 1984;170(1):29-43.
1080 33. Jain R, Shore S. External inferior colliculus integrates trigeminal and acoustic
1081 information: unit responses to trigeminal nucleus and acoustic stimulation in the guinea
1082 pig. *Neurosci Lett.* 2006;395(1):71-75.
1083 34. Lesicko AM, Hristova TS, Maigler KC, Llano DA. Connectional Modularity of Top-
1084 Down and Bottom-Up Multimodal Inputs to the Lateral Cortex of the Mouse Inferior
1085 Colliculus. *J Neurosci.* 2016;36(43):11037-11050.
1086 35. Oliver DL, Morest DK. The central nucleus of the inferior colliculus in the cat. *J Comp*
1087 *Neurol.* 1984;222(2):237-264.
1088 36. Syka J, Popelar J, Kvasnak E, Astl J. Response properties of neurons in the central
1089 nucleus and external and dorsal cortices of the inferior colliculus in guinea pig. *Exp Brain*
1090 *Res.* 2000;133(2):254-266.
1091 37. Zhou J, Shore S. Convergence of spinal trigeminal and cochlear nucleus projections in
1092 the inferior colliculus of the guinea pig. *J Comp Neurol.* 2006;495(1):100-112.
1093 38. Lehnert BP, Santiago C, Huey EL, et al. Mechanoreceptor synapses in the brainstem
1094 shape the central representation of touch. *Cell.* 2021;184(22):5608-5621 e5618.
1095 39. Berkley KJ, Budell RJ, Blomqvist A, Bull M. Output systems of the dorsal column nuclei
1096 in the cat. *Brain Res.* 1986;396(3):199-225.

1097 40. Francis JT, Xu S, Chapin JK. Proprioceptive and cutaneous representations in the rat
1098 ventral posterolateral thalamus. *J Neurophysiol.* 2008;99(5):2291-2304.
1099 41. Horne MK, Tracey DJ. The afferents and projections of the ventroposterolateral thalamus
1100 in the monkey. *Exp Brain Res.* 1979;36(1):129-141.
1101 42. Kaas JH, Nelson RJ, Sur M, Dykes RW, Merzenich MM. The somatotopic organization
1102 of the ventroposterior thalamus of the squirrel monkey, Saimiri sciureus. *J Comp Neurol.*
1103 1984;226(1):111-140.
1104 43. Mountcastle VB, Henneman E. The representation of tactile sensibility in the thalamus of
1105 the monkey. *J Comp Neurol.* 1952;97(3):409-439.
1106 44. Handler A, Zhang Q, Pang S, et al. Three-dimensional reconstructions of
1107 mechanosensory end organs suggest a unifying mechanism underlying dynamic, light
1108 touch. *Neuron.* 2023;111(20):3211-3229 e3219.
1109 45. Qi L, Iskols M, Handler A, Ginty DD. Krause corpuscles of the genitalia are vibrotactile
1110 sensors required for normal sexual behavior. *bioRxiv.* 2023.
1111 46. Saal HP, Bensmaia SJ. Touch is a team effort: interplay of submodalities in cutaneous
1112 sensibility. *Trends Neurosci.* 2014;37(12):689-697.
1113 47. Santiago C, Sharma N, Africawala N, et al. Activity-dependent development of the body's
1114 touch receptors. *bioRxiv.* 2023.
1115 48. Alvarez-Buylla R, Ramirez de Arellano J. Local responses in Pacinian corpuscles. *Am J*
1116 *Physiol.* 1953;172(1):237-244.
1117 49. Bell J, Bolanowski S, Holmes MH. The structure and function of Pacinian corpuscles: a
1118 review. *Prog Neurobiol.* 1994;42(1):79-128.
1119 50. Hunt CC, Mc IA. Characteristics of responses from receptors from the flexor longus
1120 digitorum muscle and the adjoining interosseous region of the cat. *J Physiol.*
1121 1960;153(1):74-87.
1122 51. Mountcastle VB, Talbot WH, Darian-Smith I, Kornhuber HH. Neural basis of the sense
1123 of flutter-vibration. *Science.* 1967;155(3762):597-600.
1124 52. Talbot WH, Darian-Smith I, Kornhuber HH, Mountcastle VB. The sense of flutter-
1125 vibration: comparison of the human capacity with response patterns of mechanoreceptive
1126 afferents from the monkey hand. *J Neurophysiol.* 1968;31(2):301-334.

1127 53. Luo W, Enomoto H, Rice FL, Milbrandt J, Ginty DD. Molecular identification of rapidly
1128 adapting mechanoreceptors and their developmental dependence on ret signaling.
1129 *Neuron.* 2009;64(6):841-856.
1130 54. Luo W, Wickramasinghe SR, Savitt JM, Griffin JW, Dawson TM, Ginty DD. A
1131 hierarchical NGF signaling cascade controls Ret-dependent and Ret-independent events
1132 during development of nonpeptidergic DRG neurons. *Neuron.* 2007;54(5):739-754.
1133 55. Emanuel AJ, Lehnert BP, Panzeri S, Harvey CD, Ginty DD. Cortical responses to touch
1134 reflect subcortical integration of LTMR signals. *Nature.* 2021;600(7890):680-685.
1135 56. Gottschaldt KM, Vahle-Hinz C. Merkel cell receptors: structure and transducer function.
1136 *Science.* 1981;214(4517):183-186.
1137 57. Ribot-Ciscar E, Vedel JP, Roll JP. Vibration sensitivity of slowly and rapidly adapting
1138 cutaneous mechanoreceptors in the human foot and leg. *Neurosci Lett.* 1989;104(1-
1139 2):130-135.
1140 58. Chirila AM, Rankin G, Tseng SY, et al. Mechanoreceptor signal convergence and
1141 transformation in the dorsal horn flexibly shape a diversity of outputs to the brain. *Cell.*
1142 2022;185(24):4541-4559 e4523.
1143 59. Duque D, Perez-Gonzalez D, Ayala YA, Palmer AR, Malmierca MS. Topographic
1144 distribution, frequency, and intensity dependence of stimulus-specific adaptation in the
1145 inferior colliculus of the rat. *J Neurosci.* 2012;32(49):17762-17774.
1146 60. Perez-Gonzalez D, Malmierca MS, Covey E. Novelty detector neurons in the mammalian
1147 auditory midbrain. *Eur J Neurosci.* 2005;22(11):2879-2885.
1148 61. Takada Y, Beyer LA, Swiderski DL, et al. Connexin 26 null mice exhibit spiral ganglion
1149 degeneration that can be blocked by BDNF gene therapy. *Hear Res.* 2014;309:124-135.
1150 62. Yu Q, Wang Y, Chang Q, et al. Virally expressed connexin26 restores gap junction
1151 function in the cochlea of conditional Gjb2 knockout mice. *Gene Ther.* 2014;21(1):71-80.
1152 63. Guo J, Ma X, Skidmore JM, et al. Gjb2 gene therapy and conditional deletion reveal
1153 developmental stage-dependent effects on inner ear structure and function. *Mol Ther*
1154 *Methods Clin Dev.* 2021;23:319-333.
1155 64. Lalwani AK. Evaluation of childhood sensorineural hearing loss in the post-genome
1156 world. *Arch Otolaryngol Head Neck Surg.* 2002;128(1):88-89.

1157 65. Lee MY, Takada T, Takada Y, et al. Mice with conditional deletion of Cx26 exhibit no
1158 vestibular phenotype despite secondary loss of Cx30 in the vestibular end organs. *Hear*
1159 *Res.* 2015;328:102-112.
1160 66. Xiong XR, Liang F, Zingg B, et al. Auditory cortex controls sound-driven innate defense
1161 behaviour through corticofugal projections to inferior colliculus. *Nat Commun.*
1162 2015;6:7224.
1163 67. Allen TA, Narayanan NS, Kholodar-Smith DB, Zhao Y, Laubach M, Brown TH. Imaging
1164 the spread of reversible brain inactivations using fluorescent muscimol. *J Neurosci*
1165 *Methods.* 2008;171(1):30-38.
1166 68. Arikan R, Blake NM, Erinjeri JP, Woolsey TA, Giraud L, Highstein SM. A method to
1167 measure the effective spread of focally injected muscimol into the central nervous system
1168 with electrophysiology and light microscopy. *J Neurosci Methods.* 2002;118(1):51-57.
1169 69. Kwon SE, Yang H, Minamisawa G, O'Connor DH. Sensory and decision-related activity
1170 propagate in a cortical feedback loop during touch perception. *Nat Neurosci.*
1171 2016;19(9):1243-1249.
1172 70. Sathian K. Tactile sensing of surface features. *Trends Neurosci.* 1989;12(12):513-519.
1173 71. Park JM, Hong YK, Rodgers CC, et al. Deep and superficial layers of the primary
1174 somatosensory cortex are critical for whisker-based texture discrimination in mice
1175 *bioRxiv.* 2022.
1176 72. Stuttgen MC, Schwarz C. Barrel cortex: What is it good for? *Neuroscience.* 2018;368:3-
1177 16.
1178 73. Hong YK, Lacefield CO, Rodgers CC, Bruno RM. Sensation, movement and learning in
1179 the absence of barrel cortex. *Nature.* 2018;561(7724):542-546.
1180 74. Meredith MA, Stein BE. Interactions among converging sensory inputs in the superior
1181 colliculus. *Science.* 1983;221(4608):389-391.
1182 75. Holmes NP, Spence C. Multisensory integration: space, time and superadditivity. *Curr*
1183 *Biol.* 2005;15(18):R762-764.
1184 76. King AJ, Palmer AR. Integration of visual and auditory information in bimodal neurones
1185 in the guinea-pig superior colliculus. *Exp Brain Res.* 1985;60(3):492-500.
1186 77. Matsuoka T, Ahlberg PE, Kessaris N, et al. Neural crest origins of the neck and shoulder.
1187 *Nature.* 2005;436(7049):347-355.

1188 78. Hasegawa H, Abbott S, Han BX, Qi Y, Wang F. Analyzing somatosensory axon
1189 projections with the sensory neuron-specific Advillin gene. *J Neurosci.*
1190 2007;27(52):14404-14414.
1191 79. Liu Y, Rutlin M, Huang S, et al. Sexually dimorphic BDNF signaling directs sensory
1192 innervation of the mammary gland. *Science.* 2012;338(6112):1357-1360.
1193

1194 **Acknowledgements**
1195 We thank A. Handler, H. Kwak, K. Lezgiyeva, R. Martinez-Garcia, J. Peng, K. Ng, A. Emanuel,
1196 and A. Shuster for comments on the manuscript. We thank A. Emanuel for code used for the
1197 MEA data analysis. This work was supported by a HHMI Hannah Gray fellowship (GER), NEI
1198 P30 Core Grant for Vision Research #EY012196 (OM), NIH grants F31 NS097344 (ELH) and
1199 R35 5R35NS097344-05 (DDG), and the Edward R. and Anne G. Lefler Center for
1200 Neurodegenerative Disorders (DDG). DDG is an investigator of the Howard Hughes Medical
1201 Institute. This article is subject to HHMI's Open Access to Publications policy. HHMI lab heads
1202 have previously granted a nonexclusive CC BY 4.0 license to the public and a sublicensable
1203 license to HHMI in their research articles. Pursuant to those licenses, the author-accepted
1204 manuscript of this article can be made freely available under a CC BY 4.0 license immediately
1205 upon publication.
1206

1207 **Author Contributions**
1208 ELH and DDG conceived the study. ELH did the MEA recordings in both anesthetized and
1209 awake conditions, with help from JT and MD. JT and ZKS performed primary sensory neuron
1210 recordings. ELH, AH, and MD performed anatomy and immunohistochemistry experiments.
1211 MMD, OM, and ELH developed the vibration behavioral assay. ELH did the saline and
1212 muscimol IC injections, and MMD performed behavioral experiments for vibration, temperature,
1213 and texture preference assays, with help from ELH. GER performed auditory brainstem response
1214 (ABR) measurements with guidance from LVG. KTB and DPC generated and provided the
1215 *Gjb2*$^{flox/flox}$ *Sox10*^{Cre} mice. ELH and DDG wrote the manuscript with input from all authors.